Alessandro Nazzi[1], Chiara Favaretto[2], Maurizio Corbetta[1,2,3], Michele Allegra[1,4,+]

[1] Padova Neuroscience Center, University of Padova, Padova, Italy
[2] Department of Neuroscience, University of Padova, Padova, Italy
[3] Venetian Institute for Molecular Medicine, Padova, Italy
[4] Department of Physics and Astronomy, University of Padova, Padova, Italy
[+] michele.allegra@unipd.it

Switching patterns of cortical-subcortical interaction in the human brain

ABSTRACT

Resting-state fMRI studies show that functional connectivity (FC), defined as the correlation between the blood-oxygen-level-dependent (BOLD) signals of different brain areas, undergoes rapid fluctuations, a phenomenon called dynamic or time-varying FC. Although the neural mechanisms underlying dynamic FC remain poorly understood, a recent contribution, based on a limited sample size, suggested that FC fluctuations are coordinated between cortex and subcortex, with rapidly switching FC patterns involving a dynamic reconfiguration of cortico-subcortical interactions (Favaretto et al., 2022). Here, building on the Human Connectome Project's database, we replicate those findings in a much larger cohort. Our analysis confirms that FC shifts are synchronized in cortex and subcortex, as two core subcortical 'clusters' comprising, respectively, limbic regions (hippocampus and amygdala) and subcortical nuclei (thalamus and basal ganglia) change their connectivity pattern with cortical regions. In particular, we consistently identify two FC patterns (states). State 1 is characterized by a strong opposition of task-positive (sensorimotor networks, dorsal attention network) and task-negative networks (default mode network, limbic regions), State 2 by a strong segregation between sensorimotor networks and association networks, and a positive coupling of limbic regions with sensorimotor networks. Our findings are robust with respect to changes in the preprocessing pipeline and the precise choice of cortical or subcortical parcellation, and hint at a general relevance of cortico-subcortical interactions in the generation of whole-brain spontaneous FC patterns.

INTRODUCTION

Even in absence of external stimuli and over behavior, the human brain thrives with activity (Raichle et al., 2010; Raichle et al., 2011), most of which is sub-threshold and occurs in the infra-slow frequency range (Palva and Palva., 2012). A striking feature of this spontaneous activity is that its fluctuations exhibit a well-defined spatiotemporal organization, with correlated fluctuations across the whole-brain that clearly emerge when looking at fMRI functional connectivity (FC) at rest. This phenomenon has been intensively scrutinized at the cortical level, leading to a well-established paradigm according to which activity fluctuations reflect the existence of several, canonical 'intrinsic networks' (Uddin et al., 2019). In comparison, the subcortical level has received much less attention. Yet, subcortical structures may be fundamental for the generation of spontaneous activity, as

cortical-subcortical loops are involved in most functional brain circuits according to a recent proposal (Suzuki et al., 2023). Several studies have focused on single subcortical structures, such as the thalamus (Hwang et al., 2017), hippocampus (Blessing et al., 2016) or cerebellum (Buckner et al., 2011), analyzing their connectivity with the cortex and showing that they can be subdivided into regions associated with different cortical networks. An implicit assumption of these studies is that the functional coupling between subcortical structures (or subdivisions thereof) and the cortex is fixed, or 'static'. However, FC at rest is time-varying, a phenomenon known as *dynamic functional connectivity* (dFC; Hutchison et al., 2013; Preti et al., 2017). While there is no universal agreement on the best methodology to characterize dFC, and on its meaning and causes (Lurie et al., 2020), evidence for dFC is abundant, as are results showing association between dFC and indicators of healthy and pathological cognition (Jia et al., 2014; Cohen et al., 2020). Therefore, the static picture of subcortical-cortical connectivity may hide a dynamic landscape where subcortical structures couple flexibly with cortical regions, and vice versa. Evidence in favor of this hypothesis comes from the recent study by Favaretto et al. (2022; henceforth called FA22), who investigated the fluctuations in subcortical and cortico-subcortical FC in stroke patients. FA22 observed synchronized fluctuations in cortical and subcortical FC, and identified two main 'blocks' of highly synchronized subcortical structures (one comprising hippocampus and amygdala, the other thalamus and basal ganglia) that alternate between different patterns of connectivity with cortical networks. These findings suggested that cortico-subcortical interactions may be relevant for the dynamic reorganization of whole-brain FC, hinting at their general relevance in the emergence of whole-brain spontaneous activity patterns.

Hare we build on FA22''s results and analyze dFC and cortico-subcortical interactions in a wide cohort of healthy young participants, made available by the Human Connectome Project (Smith et al., 2013). The large sample size (N=1200) and fine temporal resolution (0.71 s) allow for a statistically reliable characterization of dFC, reducing instabilities due to individual variability, sampling variability, and artifacts. We wish to test several hypotheses, suggested by the FA22. First, we hypothesize the existence of synchronous connectivity shifts in cortex and subcortex, captured by different connectivity states or 'dynamic functional states'. Second, we expect a split of subcortical structures into two groups characterized by internal synchronization and dynamic links with cortical networks. Third, in the light of previous work on the relationship between dFC and behavior, we conjecture that individual markers of cortical-subcortical dFC may contribute to explaining inter-individual variability in cognition. Finally, we assume that our findings will be robust with respect to details of the analysis pipeline used, including specific choices of cortical/subcortical parcellations.

MATERIALS AND METHODS

Washington dataset

All subjects included in FA22 were scanned with a 3T Siemens Tim-Trio scanner at the Washington University School of Medicine with a standard 12-channels head coil. They were divided into four experimental groups: three groups of stroke patients, depending on the time they were scanned after stroke onset (1-2 weeks, 3 and 12 months after) and one

age-matched control group. Pulse sequence included a gradient-echo EPI sequence with TR=2s acquiring 32 contiguous 4 mm slices, with 4x4 mm in-plane resolution while fixating on a small white crosshair. Pre-processing included: regression of head motion, signal from ventricles and Cerebrospinal fluid, signal from white matter, global signal; temporal filtering retaining frequencies between 0.009 and 0.08 Hz; frame censoring, with framewise displacement of 0.5 mm. After all the pre-processing steps, a total of 20 controls and 47 patients with first-time strokes were considered for the analysis (patients were scanned at three different time points: 2 weeks, 3 months, and 12 months).

Human Connectome Project dataset

The HCP's dataset included 1206 participants, who underwent neuroimaging sessions and a large battery of behavioral tests. Of the 1206 participants, 1096 were scanned with a modified 3T Siemens "Connectome skyra" scanner at the Washington University, using a standard 32-channels Siemens receive head coil and a specifically designed "body" transmission coil. Pulse sequence included slice-accelerated multiband acquisition with a multiband factor of 8, spatial resolution of 2 mm isotropic voxels and TR=0.7s. Participants underwent two 15-minutes scanning sessions with opposite phase encoding directions (L/R and R/L), while fixating on a crosshair. We included in the analysis only participants that were scanned both in the L/R and in the R/L direction for 840 s (n=1078). We used pre-processed data provided by the HCP. The HCP's preprocessing pipeline is divided into two distinct protocols (Glasser et al., 2013): one applied entirely on the volume data involving temporal filtering and de-noising and the second one regarding mapping the data to cortical surfaces and subcortical gray-matter domains using the Connectivity Informatics Technology Initiative file format (CIFTI). One promising approach for removing structured artifacts involves denoising each 15-minutes rfMRI scan with the Independent Component Analysis (ICA) based tool called FSL's MELODIC. This tool, paired with the FMRIB'S ICA-based X-noise filter, allows decomposing the data into multiple components (comprising a spatial map and a corresponding time course) and to classify them in order to subsequently regress out the confounding ones. Additionally, in line with FA22, we included two supplementary pre-processing steps: signals were band-passed in the frequency band [0.009 Hz,0.08 Hz] with a Butterworth filter of order 1 and the mean GM signal was linearly regressed (global signal regression).

Parcellations

For our initial analysis, we used the same parcellation used in FA22. Time series were projected on the cortical surface of each subject divided according to the resting state functional connectivity boundary mapping developed by Gordon et al. (2016). This technique leverages abrupt transitions in resting-state functional connectivity (RSFC) to noninvasively identify the borders separating cortical areas. The original parcellation includes 333 regions, but all regions with <20 vertices (~50 mm2) were excluded due to low signal-to-noise ratio (SNR) (Siegel et al., 2016). The remaining 324 regions were further reduced to 71 by a clustering procedure (Favaretto et al., 2022) and grouped into 8 resting state networks (RSNs): Visual Network (VIS), Sensory Motor Hand-Mouth Network (SMN), Auditory Network (AUD), Control or Cingulo-Opercular Network (CON), Ventral Attention Network (VAN), Dorsal Attention Network (DAN), Fronto Parietal Network (FPN), Default Mode Network (DMN), Limbic Network (LIM). We also considered 19 subcortical and cerebellar

regions derived from the FreeSurfer subcortical atlas (Fischl 2012; Fischl et al., 2002). Expanding the initial analysis to aid the investigation of cortico-subcortical interactions, we used a different parcellation of the subcortex (Tian et al., 2020). Tian et al. (2020) provide four different parcellations of the subcortex with an increasing degree of granularity. The coarsest parcellation includes 8 bilateral regions, while the most fine grained one comprises 27 bilateral regions (see Supplementary Table 2 of Tian et al., 2020). This subcortical cartography was based on resting state functional connectivity gradients ("gradientography"): region boundaries were identified on the basis of strong shifts in functional connectivity gradients. To analyze the cerebellum, we considered the cerebellar parcellation by Buckner et al. (2011). This parcellation was obtained by considering the resting-state FC between the cerebellum and the cortex. In particular, the cortex was divided into seven RSNs (according to Yeo et al., 2011), and the FC between each voxel in the cerebellum and each cortical RNS was assessed; based on the maximal FC, cerebellum voxels were assigned to one of seven clusters based on their maximum correlation with cortical regions. Finally, we considered an anatomical parcellation of the thalamus ('Morel atlas') provided by Krauth et al. (2010). This map was obtained from detailed histological maps of the thalamus.

Sliding-window functional connectivity

FC dynamics were investigated through sliding window temporal correlation, one of the most straightforward approaches for dynamic FC analysis. Similarly to a moving average function, this technique computes a succession of pairwise Fisher z-transformed Pearson correlation matrices, relative to windows of a given width. These correlation matrices are informative of the time-varying FC between the networks considered in the brain parcellation of choice. Importantly, to compensate for the difference in TR durations between the two datasets (i.e., FA22's TR=2 s and HCP's TR=0.7 s), we down-sampled HCP's timeseries to one third of the points. Then, from the down-sampled timeseries, we extracted windows lasting approximately one minute (28 TRs), with a sliding step of 3 TRs (approximately 2 s). Window-length choice represents a critical point in dynamical functional connectivity analysis (Leonardi and Van De Ville, 2015). Namely, having windows shorter than the analyzed components' wavelengths might cause spurious fluctuations in dynFC. Similarly, too long windows might prevent legitimate functional fluctuations to be identified. Thus, we selected our sliding window's width on the basis of previous results, matching FA22's choice. Additionally, each correlation matrix was approximated by projecting it onto the corresponding eigenspace, defined by the first eigenvector v_i. Since eigenvectors are defined less than the sign, we averted this problem by translating each eigenvector into the reconstructed square matrix $v_i \times v_i^t$, saving the vectorized upper-triangular part alone, avoiding redundancies in the data. Ultimately, all the resulting vectors were concatenated across windows, subjects, and time points.

Dynamic Functional States' definition

The last step for DFS's definition required the application of a time-wise K-means clustering procedure with correlation distance. K-means is a clustering technique, aiming to partition an N-dimensional population into k clusters based on a sample. Each observation belongs to the cluster with the nearest mean (e.g., cluster centroid), serving as a prototype of the cluster, resulting, in this case, in a set of five Dynamic Functional States (all the operations

described up to now are summarized in Fig. 1b). This algorithm minimizes within-cluster variances, taking into account a range of possible distance metrics. For this analysis, we employed the correlation distance, which is defined as follows:

$$d(x,c) = 1 - \frac{(x-\bar{x})(c-\bar{c})'}{\sqrt{(x-\bar{x})(x-\bar{x})'}\sqrt{(c-\bar{c})(c-\bar{c})'}}$$

Where: x is an observation and c is a centroid. In addition, $\bar{x} = \frac{1}{p}(\sum_{j=1}^{p} x_j)\vec{1_p}$, $\bar{c} = \frac{1}{p}(\sum_{j=1}^{p} c_j)\vec{1_p}$ and $\vec{1_p}$ is a row vector of p ones. Furthermore, the optimal K value was deducted by comparing the clustering performances with different numbers of clusters (from 2 to 10), with respect to a metric for interpreting and validating the consistency within clusters of data: the Silhouette value. This parameter is a measure of the fitness of a certain data point for its cluster of belonging, compared to other clusters. This metric ranges from -1, indicating the lowest fitness and +1, indicating the highest fitness. Then, for a certain data point $i \in C_I$, where C_I is the cluster of belonging, the Silhouette value is defined as follows:

$$s(i) = \frac{b(i)-a(i)}{max\{a(i),b(i)\}},\ if\ |C_I| > 1$$

Where, $a(i)$ is the mean distance between i and all the other data points belonging to the same cluster, while $b(i)$ is the smallest mean distance between i and all the data points belonging to other clusters.

Each DFS was classified with three indices commonly employed as static FC biomarkers in stroke, namely: the average homotopic inter-hemispheric connectivity within each network (i.e., the average connectivity between homologous regions of different hemispheres forming a network); the average intra-hemispheric connectivity between Dorsal Attention network (DAN) and Default Mode Network (DMN), as a measure of network integration; and the overall Newman's modularity among cortical networks.

Additionally, the clustering procedure associated each sliding window to a specific DFS, so that for each subject we had a discrete time series $x(n)$ (with n ranging from 1 to 746), where each value represented the active Dynamic Functional State for that time window. These time courses allowed us to evaluate three dynamical measures for each state, namely: fraction time f_k, being the percentage of times during which a state is active:

$$f_k = \frac{\#(x(n)=k)}{746}, k = 1,..., K$$

where $\#(a)$ stands for the number of occurrences of the condition a. The dwell time l_k, being the average length of periods in which each state remains continuously active:

$$l_k = \frac{1}{|L_k|}\sum_{i=1}^{|L_k|} L_k[i]$$

where L_k is the set having cardinality $|L_k|$, with each element $L_k[i]$ representing the length of a period of continuous activity of state k. The transition probability $DFS_i > DFS_j$, from DFS_i to DFS_j, where:

$$DFS_i > j = \frac{\#(x(n=i) \wedge x(n+1)=j)}{\#(x(n) \neq x(n+1))}$$

being the ratio between the number of jumps from DFS_i to DFS_j over the total amount of jumps.

Phase randomization

Phase randomization (PR) is a common framework for generating null data extensively employed in physics (Prichard and Theiler, 1994). Recently, it has also been applied to fMRI data for studying dynamic FC (Allen et al., 2014; Hindricks et al., 2016). The PR procedure performs a Discrete Fourier Transform (DFT) of the original time series, adds a uniformly distributed random phase to each frequency, and then performs the inverse DFT to create surrogate data. Crucially, the random phases are created individually for each frequency, but they remain consistent across various regions of the brain. Adding the same random phase to the same frequency components of the RSNs preserves the static FC and the lagged cross-covariance structure in the surrogates (in addition, also the mean, variance and power spectrum of the signals are preserved). This class of surrogates correspond to the null hypothesis that time series are generated by a linear, stationary Gaussian process (Liégeois et al., 2017).

Behavioral analysis

The HCP provides a large array of subject measures (SMs; i.e. individual measures for each participant), covering demographic, psychometric and behavioral information. The full list of SMs with a detailed description can be found in the HCP 1200 Manual. SMs comprise demographics (e.g., education, employment, income); physical and mental health history, present and past use of tobacco, alcohol, marijuana, and other drugs; Symptoms/history of eating disorders, depression, psychosis, antisocial personality, obsessive-compulsive disorder, post-traumatic stress, social phobia, panic attack; Folstein MiniMental State Exam; Pittsburgh Sleep Quality Index; Parental Psychiatric and neurologic history; Handedness assessment; Menstrual cycle and other endocrine information in females; Urine drug assessment, breathalyzer test, Blood test; NIH Toolbox behavioral tests (which includes 19 sub-domains within the broad domains of cognitive, motor, emotional and sensory functions); Non-NIH Toolbox behavioral tests (color vision, contrast sensitivity, personality, attention, episodic memory, fluid intelligence, emotion processing, spatial processing, and delay discounting)

Starting from a subset of 158 of such SMs, Smith et al. (2015) performed a canonical correlation analysis (CCA) linking the SMs with the individual static FC matrices, which resulted in a principal axis of FC-SM co-variation. They list 59 SMs (listed in Supp. Inf.) with a large loading onto the principal axis. We replicated the analysis by Smith et al. (2015) using the same methodology. However, we used a larger cohort of subjects from the HCP database (i.e. 1206 vs 461 HCP subjects), and we computed connectivity matrices in the Schaefer100 + Freesurfer cortico-subcortical parcellation (while Smith et al. used a

customized functional parcellation with 200 regions). The raw behavioral measures for the selected 158 SMs were initially subject to a rank-based inverse Gaussian transformation to enforce Gaussianity, avoiding the influence of potential outliers. Additionally, 17 potential confound SMs (including head motion) were regressed out from the behavioral data (for a complete list see Smith et al. 2015). To account for missing data, a subjects x subjects covariance matrix was estimated by ignoring missing values for either subject, which was then projected onto the nearest valid positive-definite covariance matrix. Finally, the eigenvalue decomposition was computed onto the resulting covariance matrix, and the first 100 eigenvectors were kept. Regarding connectivity data (referred as N), we computed subject-wise partial temporal correlation between the time series of each region keeping only the upper-triangular part of each correlation matrix. The resulting vectors were concatenated across subjects and the Pearson correlation values transformed into z statistics with Fisher's transformation. Then, this connectivity matrix was demeaned column-wise, globally variance-normalized and the same confounds SMs were regressed out. Lastly, a principal component analysis was computed on N, keeping the first 100 components. The fully preprocessed behavioral and connectivity matrices (S and N respectively) were ultimately fed into a CCA, identifying 100 components aiming to optimize de-mixing matrices A and B to ensure that the resulting matrices $U = N\,A$ and $V = S\,B$ were highly similar to each other.

Granziol and Cona (2023) analyzed 38 SMs reflecting cognitive and processing aspects, mental health and behavioral problems, personality characteristics, and substance use frequencies (the list of the 38 SMs is reported in Supp. Inf.). Exploratory Graph Analysis (EGA; Golino and Epskamp, 2017) was used to cluster these SMs into "communities" or clusters of SMs characterized by high correlation. Briefly, EGA works with the following steps: i) the graphical LASSO algorithm (Friedman et al., 2008) was used to find partial correlations between the 38 SMs ii) the walktrap community detection algorithm (Pons and Latapy 2005) is applied to find clusters/communities. Seven domains were identified (mental health, substance abuse, low cognitive functions, high cognitive functions, pain, delay discounting, externalizing problems).

We replicated the analysis by Granziol and Cona (2023) using the graphical LASSO algorithm with sparsity 0.5, as implemented in the R package 'glasso'; we then applied the walktrap community detection as implemented in the R 'igraph' package. We computed network loadings for each measure as follows (Christensen et al., 2019): starting from the partial correlation matrix W_{ij}, where $i, j = 1, \cdots, N_{SM}$, we considered all SMs assigned to factor c and computed loading as $L_{ic} = \sum_{i \in c} |W_{ij}|$ and then we normalized loadings as $z_{ic} = \frac{L_{ic}}{\sum_j L_{jc}}$. Given the set of SMs for all subjects, X_{ik} where $k = 1, \cdots, N_{subjects}$, we computed community/cluster scores for each subject as $S_{ck} = \sum_i z_{ic} X_{ik}$ (Granziol and Cona 2023; Christensen et al, 2019).

Ultimately, we assessed the impact of variability in dFC patterns via a Generalized Linear Model (GLM) in an exploratory analysis considering different predictors (fraction times, dwell times, P(jump in area1|jump in area2) and individual DFSs) and the two behavioral scores described above (i.e. Smith's behavioral mode and Granziol's 7 communities scores) as alternative dependent variables.

RESULTS

Analysis overview

We considered a large sample of healthy human subjects (n=1078) from the Human Connectome Project database (Van Essen et al., 2013; Smith et al., 2013). For each subject, we extracted average functional time series for all regions of an atlas comprising 71 cortical regions (obtained by clustering together functionally homogeneous parcels in the Gordon-Laumann atlas) and 19 subcortical and cerebellar regions from the Freesurfer atlas. We computed functional connectivity (FC) matrices for sliding windows with a 60s duration projected them onto the space spanned by the principal eigenvector, and vectorized them; we then concatenated together all time windows and subjects and performed a K-means clustering over windows. The resulting clusters are termed *dynamic functional states (DFSs)*.

In Fig. 1, we summarize the main idea and goal of the present study. In Fig. 1a we show the average BOLD signal of two cortical networks (the default mode network and the sensorimotor network) and two subcortical regions (thalamus and hippocampus) affiliated respectively to the two main subcortical groups (see FA22 and Fig. 4) SC1 (thalamus/basal ganglia) and SC2 (hippocampus/amygdala). Starting from sliding-window functional connectivity (swFC), we extract the DFSs (Fig. 1b). Two stable DFSs correspond to different cortical-subcortical interactions. This is evident in Fig. 1d, where we show the values of swFC in time windows associated with the different DFSs. In DFS1, task-negative regions correlate positively with SC2 and negatively with SC1, while the opposite pattern is observed for task-positive regions. In DFS2, this trend is reversed, as task-negative regions correlate negatively with SC2 and positively with SC1, while the opposite pattern is observed for task-positive regions.

Existence of two groups of subcortical regions

A key finding in FA22 was the identification of two groups of subcortical regions exhibiting anticorrelated FC fluctuations: a first group ('subcortical group 1', 'SC1') comprising hippocampus and amygdala, and a second group ('subcortical group 2', 'SC2') comprising thalamus, basal ganglia and cerebellum. These two groups were identified by performing a principal component analysis (PCA) on dFC, i.e., a PCA on the subcortical projection of v (the first principal eigenvector of the windowed FC, of which we consider entries corresponding to subcortical regions). The rationale behind this analysis was that v can be thought of as a 'condensed' representation of the windowed FC. Consequently, performing a PCA on the subcortical projection of v allows identifying subcortical regions having similar *fluctuations* in windowed FC across time (windows).
Two main PCs were found, projecting respectively on SC1 and SC2. We replicated this dFC-PCA analysis in the HCP data set. Identifying a main principal component (PC1), explaining 34% of the total variance (Fig. 2a) [2nd component: 14%; 3rd component: 7%; all other components < 4%]. PC1 loaded positively on cerebellum, thalamus, putamen, caudate (bilaterally) and the brain stem; it loaded negatively on hippocampus, amygdala, nucleus accumbens (bilaterally) and had weak loadings on globus pallidus and diencephalon

(bilaterally). PC1 is also displayed in a volumetric brain representation in Fig. 2b. This principal component aligned with the subcortical cluster division identified by FA22, as it loaded mostly positively on regions identified as SC1 in FA22, and mostly negatively on the majority of regions identified as SC2 in FA22. Using PC1 loadings, we can thus obtain a division of the subcortex and cerebellum into two groups, which we also term SC1 and SC2. The alignment between subcortical groups found in ou study and in FA22 is strong but not full, as there are two discrepancies: globus pallidus was included in SC1 in FA22, but it could not be included in either SC1 or SC2 in our study (it exhibits a weak loading on PC1); the nucleus accumbens was not included in either SC1 or SC2 in FA22, while it was included is SC2 in our study (loading negatively on PC1). However, the main split thalamus/basal ganglia vs limbic regions (hippocampus/amygdala) is strongly confirmed by our replication study.

We further asked whether a more fine-grained parcellation would not lead to a more nuanced picture, particularly for the thalamus and cerebellum that are taken as compact regions in the Freesurfer parcellation, but are well known to have important structural and functional subdivisions. Therefore, we repeated the dFC-PCA analysis with different subcortical parcellations. In Fig. S1 2b, 2c we report the results obtained using two subcortical parcellations proposed by Tian et al. (2019), one with 8 bilateral regions ('TianS1') and the other with 27 bilateral regions ('Tian S4') (among the four parcellations proposed by Tian et al., which are mutually consistent but correspond to different granularity levels, we restricted attention to the coarsest and the finest parcellation). The Tian S1 parcellation roughly aligns with the Freesurfer parcellations, but it excludes some regions (cerebellum, brainstem, and diencephalon) and it splits the thalamus in an anterior and posterior portion. Using this parcellation, we find a main principal component explaining 33% of the variance [2nd component: 15%; 3rd component: 8%; 4th component: 6%, all other components < 5%]. PC1 loaded positive. Results of the dFC-PCA analysis are consistent with those obtained with the Freesurfer parcellation, with two main differences. Firstly, the nucleus accumbens is no longer associated with SC2, as it exhibits weak values of PC1. This outcome is more consistent with FA22. Moreover, we find a neat split of the thalamus: its anterior portion is strongly associated with SC1, while the posterior portion has weak values of PC1, and it cannot be clearly included in either SC1 or SC2. The Tian S4 parcellation provides subdivisions of Tian S1 regions: the anterior thalamus is split into 5 regions, the posterior thalamus into 3 regions, the caudate into 4 regions, the putamen into 4 regions, the globus pallidus into 2 regions, the hippocampus into 5 regions, the amygdala into 2 regions, and the nucleus accumbens into 2 regions. Results of the dFC-PCA analysis are fully consistent with those obtained with Tian S1. We found a main PC (PCQ1) explaining 24% of the total variance [2nd component: 8%, 3rd component: 5%, all other components < 4%]. PC1 loads positively on regions of the anterior thalamus, caudate and putamen; negatively on regions of the hippocampus and amygdala; and weakly on regions of the nucleus accumbens, posterior thalamus and globus pallidus. In other words, the finer subdivisions of subcortical regions offered by Tian S4 do not alter or complexify the picture obtained with Tian S1.

To further confirm the split between the anterior and posterior portion of the thalamus, we additionally considered the anatomical thalamus subdivision provided by Krauth et al. ('Morel atlas'; 2010), which provides divisions of the thalamus into nuclei, with several granularity levels. At the coarsest level, the thalamus is split into 7 bilateral portions: medial nuclei, posterior nuclei, lateral nuclei, anterior nuclei, red nucleus, mammillothalamic tract and subthalamic nucleus. We thus combined the Tian S1 parcellation with the Morel atlas

(replacing the anterior/posterior thalamus in Tian S1 with the 7 regions of the Morel atlas, and maintaining the other subcortical regions as given in Tian S1). Results of the dFC-PCA analysis are consistent with those obtained with Tian S1. We found a main principal component explaining 28% of the total variance [2nd component: 10%, 3rd component: 6%, all other components < 4%]. In particular, PC1 loads positively on the medial, lateral and anterior regions of the thalamus, and more weakly on the posterior regions and the additional nuclei (Fig. S1).
Finally, we considered a possible subdivision of the cerebellum. To this aim, we used the cerebellar atlas provided by Buckner et al. (2013), who split the cerebellum into 7 regions, each of which is associated (by strong values of static FC) with one of the seven cortical RSNs identified in the classical study by Yeo et al. (2013). We combined the Tian S1 parcellation with the Buckner atlas (adding cerebellar regions to the Tian S1 regions). Results of the dFC-PCA analysis are consistent with those obtained with the Freesurfer parcellation and Tian S1. In particular, PC1 loads positively on anterior regions of the thalamus, and more weakly on the posterior regions and the additional nuclei (Fig. S1).
This component is very robust and found independently of the specific subcortical parcellation used (Freesurfer, Tian S1, Tian S4).

Coordination of cortical and subcortical connectivity shifts

Another key finding in FA22 was the general coordination between cortical and subcortical connectivity shifts. This was reflected in a higher-than-chance conditional probability to have an 'FC jump' (change of windowed FC above a fixed threshold) in cortical regions, provided that a similar jump occurs in subcortical regions, and vice versa. More precisely, we computed the average windowed FC within each RSN (by approximating the FC with its first eigenvector and taking the average of the absolute values within each RSN), and computed an RSN-wide FC change as the difference between two successive windows. We identified an 'FC jump' whenever this difference falls in the upper tail of the corresponding distribution (5th percentile). Finally, we computed conditional probabilities p(RSN1|RSN2) of observing an FC jump in RSN1, given that a jump is observed in RSN2. In Fig. 2e we show the matrix of conditional probabilities. All probabilities are >50%, implying that FC jumps are strongly synchronized among different regions. In particular, cortical jumps are synchronized with subcortical jumps. Notably, cortical jumps and subcortical jumps are synchronized, with conditional probabilities involving cortical networks and subcortical groups being all >60%. In particular, among the strongest conditional probabilities are those involving simultaneous jumps between SC1 (basal ganglia/thalamus) and cortical networks.

Dynamic functional states

In Fig. 3a, we plot the average silhouette value as a function of the chosen number of clusters K. The 'optimal' number of clusters should correspond to the largest silhouette value. In the HCP data, the average silhouette is a monotonically decreasing function of K, with K=2 emerging as the best choice for the number of clusters. In Fig. 3b,3d we show the two states found when fixing K=2 for the GordonLaumann+FreeSurfer parcellation. States are shown both in a matrix representation, and in a brain representation including a surface (cortical) and a volume (subcortical) visualization of the cortico-subcortical interaction, captured in brain surface/volume maps. The matrix representation shows the division of regions into seven resting state networks (RSNs) according to Gordon et al. (2016),

including the visual network (VIS), the sensorimotor network (SMN), the auditory network (AUD), the dorsal attention network (DAN), cingulo-opercular network (CON), ventral attention network (VAN), the frontoparietal network (FPN), and the default mode network (DMN).

DFS1 displays high DAN/DMN segregation, positive limbic-DMN connectivity and negative limbic-DAN connectivity, closely resembling the typical pattern of healthy static FC. DFS2 presents a significant DAN/DMN integration, negative limbic/DMN connectivity and a negative coupling between cognitive clusters and sensorimotor clusters. These two states capture the competitive relationship between basal ganglia/thalamus (SC1) and limbic nuclei (SC2), with DFS1 showing a positive correlation between DMN and SC2 and DFS2 showing the opposite FC pattern. Additionally, DFS1 maintains a FC profile similar to healthy static FC. The correlation between cortical and subcortical regions in the two states is summarized in Fig. 3c.

We tested the robustness of our results with respect to the choice of K, performing clustering with variable K (from 2 to 6). As typical for K-means, as K grows, the most robust clusters survive, while others progressively split into subclusters with more and more fine grained structure. In Supp. Fig. S5 we show the states for all K, showing that the states found at K=2 are robustly preserved across the whole range of K values.

We compared results for K=5 with the 5 states originally found by FA22 in the Washington University data set ('WU'). We only partially replicate the patterns found in the previous study. Fig. S6 shows a confusion matrix representing the similarity of the K=5 states previously found by FA22 in the Washington data set and the states found in the HCP data set ('HCP'). Similarity is assessed by the correlation between the state centroids. The DSF1 (WU) is approximately reproduced by the DFS1 (HCP), the DFS3 (WU) is partially reproduced by the DFS2,DFS3,DFS4 (HCP), while DSF2, DFS4 DFS5 (WU) are not well replicated by any of the DFS (HCP). Notbaly, DFS2 and DFS4 (WU) were particularly common in stroke patients at the acute stage, showing abnormal integration of cortical connectivity. Comparable fraction times and dwell times are observed for both data sets. In detail, we observe that the DSF1 (WU) is approximately reproduced by the DFS1 (HCP), with a correlation of 0.84. This state corresponds to the DFS1 found with K=2. The DFS3 (WU) is partially reproduced by the DFS1 and DFS2 (HCP), with correlation values of 0.65 and 0.68 of correlation respectively. These states correspond to the DFS1 found with K=2. DFS4 (WU) resembles (the correlation value is 0.46) the DFS2 (HCP), as they both show a weak cortico-subcortical connectivity. DSF2 and DFS5 (WU) could not be associated with any of the DFSs found in HCP.

We tested the robustness of the K=2 analysis with respect to preprocessing and parcellation steps. We replicated the analysis by changing the cortical and subcortical parcellation used. For a different cortical parcellation, we used the well-known Schaefer atlas with 100 regions (Schaefer et al., 2018). For the Schaefer atlas, regions are divided into RSNs according to the classification by Yeo et al. (2011), where the control network (CON) includes regions associated to the frontoparietal network by Gordon et al. (2016), and the VAN includes regions associated to the cingulo-opercular network by Gordon et al. (2016). For a different subcortical parcellation, we used the subcortical atlas provided by Tian et al. (2019). Note that this atlas does not include cerebellar regions. In Fig. S6 we show the results of changing

cortical and subcortical parcellation, respectively. We can see that the core structure of the DFS (K=2) is preserved across the parcellation changes. In particular, DFS1 is characterized by a strong DAN-DMN anticorrelation, while the hippocampus couples positively with the DMN and negatively with the task positive networks (DAN and primary networks). Conversely, DFS2 is characterized by a strong segregation of the primary networks from the association networks. Hippocampus/amygdala (SC2) correlate positively with primary networks and negatively with association networks, while the opposite pattern is observed for thalamus/basal ganglia (SC1).

Next, we investigated the impact of specific preprocessing steps. We first addressed the impact of the temporal downsampling step (used to match the TR of previous studies, TR=2). Downsampling had virtually no effect on the clustering results (Fig. S3). We then tested the impact of global signal regression (GSR). Omitting GSR produced a substantial change in the structure of DFSs (Fig. S2). Thus, GSR has a sharp effect on the structure of DFSs.

Finally, to test whether the lagged cross-covariance structure of the data is sufficient to yield the observed DFSs, we applied phase randomization (PR). PR generates surrogate data that preserve the empirically measured cross-covariances but are linear and Gaussian (Liegeois et al., 2017). As shown in Fig. S4, DFSs resulting from the PR-generated time series closely resemble the ones obtained with the original data. This correspondence is furtherly investigated in the confusion matrix represented in Fig. S4b. The latter shows a neat one-to-one correspondence between the two sets of clusters, with very similar centroids.

Correlation with behavior

We tested a possible correlation between individual dynamic FC metrics and individual behavioral traits. To this aim, we summarized the large array of behavioral variables ("subject measures") available in the HCP data set into a few general descriptors capturing key aspects of cognition and behavior (Fig. 4a). In particular, we used the positive-negative mode (PNM) of behavior-FC covariation identified by Smith et al. (2015), which is a single indicator of global behavioral/social function (Methods). In addition, we considered seven individual markers identified in the recent study by Granziol and Cona (2023), which capture different aspects of cognition (Fig. 4a).

We first tested whether the average fraction of the total time, and the average time each subject spends in each DFS was predictive of their behavior. Therefore, we tested for correlation between behavioral metrics and individual fraction times/dwell times obtained with K=2. We performed a linear regression using the behavioral metrics as dependent variables and the fraction/dwell times as predictors. The total regression R^2 was always lower than 0.01, meaning that fraction/dwell times explain less than 1% of the variation in the behavioral metrics considered (Fig. 4b). We thus found no significant effect of fraction/dwell times on behavioral metrics (permutation test on R^2, corrected for 32 comparisons).

In addition, we tested whether the probabilities of synchronized jumps between cortical regions and the two main subcortical clusters could predict behavior. To this aim, we averaged the conditional probabilities (Fig. 2) by aggregating cortical regions, regions belonging to SC1, and regions belonging to SC2, obtaining a 3 x 3 matrix of synchronized jumps. From this matrix we extracted four entries corresponding to the probabilities of synchronized jumps between the cortex and, respectively, SC1 and SC2. We performed a

linear regression using the behavioral metrics as dependent variables and these probabilities as predictors. The total regression R^2 was always lower than 0.01 and non significant (Fig. 4b).

In addition, we tested whether the average FC patterns in each DFS could predict behavior. To this aim, we computed an average DFS pattern for each individual subject, by averaging the sw-FC over time windows assigned to one of the K=2 DFSs (Fig. 4c). This can be considered as a DFS pattern 'adjusted' to each participant. We averaged the FC patterns by aggregating task-positive regions (SMN, DAN, VIS), task-negative regions (CON, DMN), regions belonging to SC1, and regions belonging to SC2, obtaining two 4 x 4 matrices (one for each DFS) for each participant. We performed a linear regression using the behavioral metrics as dependent variables and the entries of this matrix as predictors. The total regression R^2 was significant for the PNM, which displayed $R^2 = 0.07$, with a significant effect ($P=0.003$, permutation test on R^2 , corrected for 32 comparisons). Higher values of the PNM are associated with higher segregation within the cortex, and between the cortex and SC1 in DFS1; and, conversely, higher integration within the cortex, and between the cortex and SC1 in DFS2 (Fig. 4d).

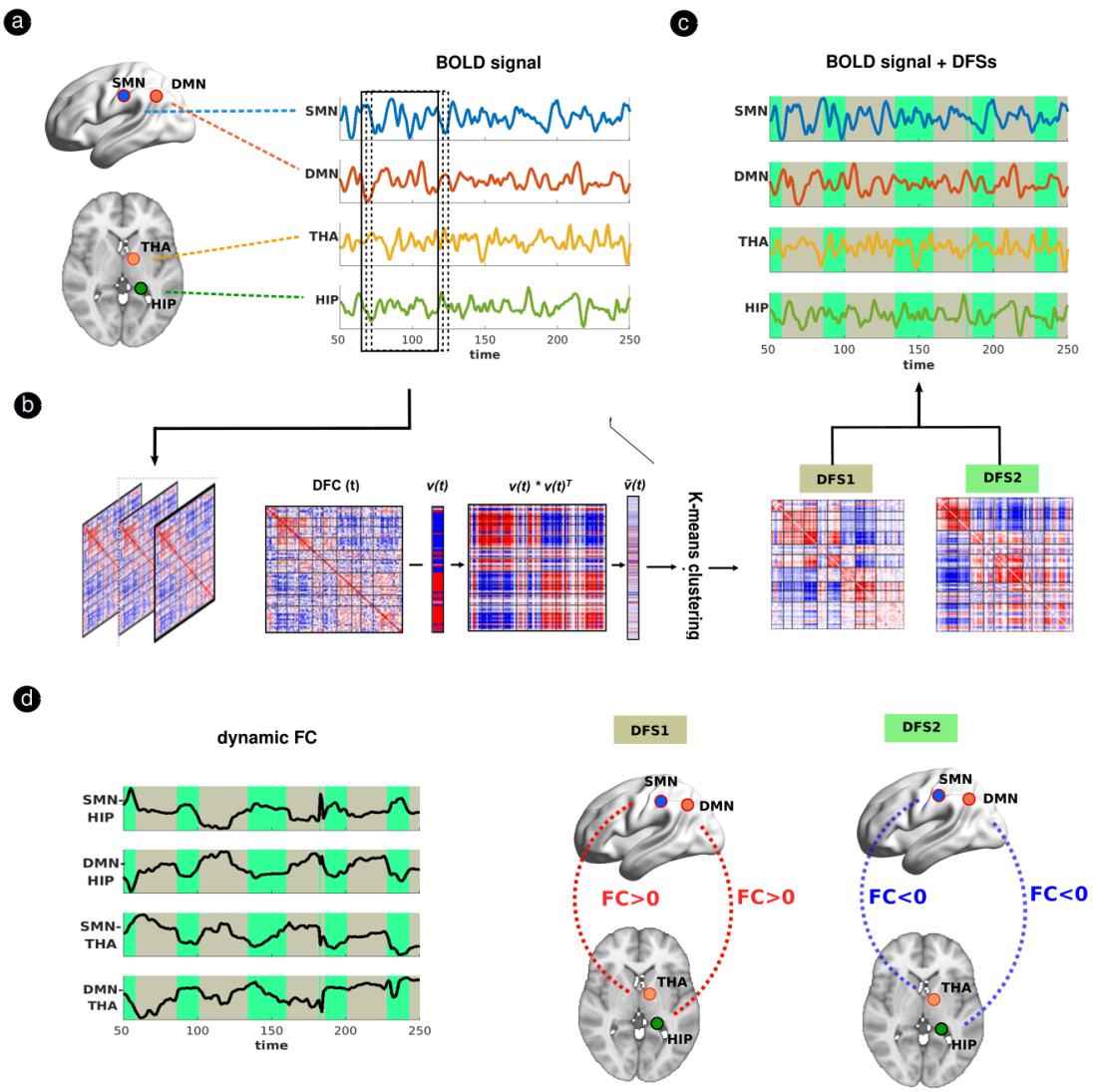

Fig. 1. Analysis overview. *This work focuses on dynamic cortico-subcortical interactions. As shown by FA22, two groups of subcortical regions (a 'limbic' group comprising hippocampus/amygdala and a 'subcortical nuclei' group comprising thalamus/basal ganglia) couple dynamically with cortical regions, showing flexible connectivity with task-positive regions (sensorimotor/dorsal attention network) and task-negative regions (default mode network). Connectivity switches are well captured by 'dynamic functional states' (DFSs), i.e., recurring patterns of whole brain (cortical-subcortical) connectivity.* ***(a)*** *(Average) BOLD signal from four regions belonging respectively to the sensorimotor network, the default mode network, the limbic group and the subcortical nuclei group for an example subject.* ***(b)*** *Overview of the analysis pipeline. Sliding window functional connectivity (swFC) is computed using sliding windows of 60 s duration (with a step of 3 s). Then, each swFC matrix is approximated as* $v_i \times v_i^t$*, by projecting on the leading eigenspace defined by the first eigenvector* v_i*. The upper triangular part of these swFC matrices is vectorized and concatenated across windows and subjects, in order to finally apply a timewise K-means clustering algorithm with correlation distance to identify a set of recurring swFC patterns or DFSs. Each sliding window is assigned to a specific DFS.* ***(c)*** *BOLD signal of four key regions (same as in panel a), with different colors highlighting the DFS of the corresponding*

window (the window centered at that point). Two DFSs capture the dynamic coupling between subcortical and cortical regions. In particular, in DFS1 the hippocampus couples positively with the default mode network and negatively with the sensorimotor network, while the thalamus shows an opposite trend. In DFS2, this pattern of subcortical-cortical connectivity is reversed ***(d)****. Time courses of the subcortical-cortical swFC, shaded with different colors according to the corresponding DFSs. The dynamic coupling described above can be noted: switching trends of subcortical-cortical connectivity are summarized graphically in the brain plots on the right.*

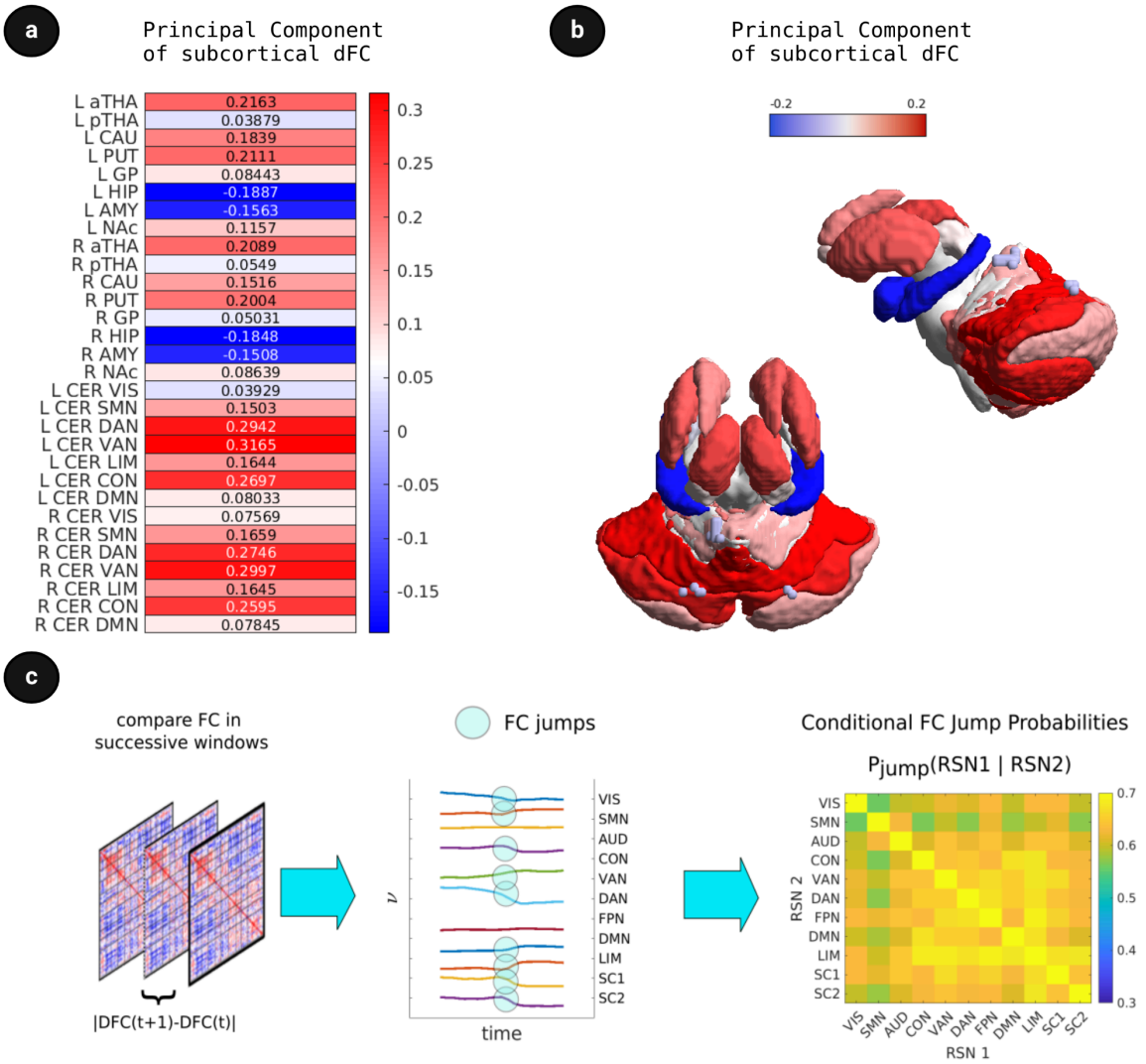

Fig. 2. Existence of two main clusters of subcortical regions *We applied PCA on the time evolution of v (principal eigenvector of the sliding-windows FC), restricting attention to subcortical regions* ***(a)*** *The first PC shows the competitive relationship between two different subcortical clusters: SC1, which includes the basal ganglia, thalamus and cerebellum, and SC2, which includes the limbic nuclei. CER: cerebellum; THA: thalamus; CAU: caudate nucleus; PUT: putamen; GP: globus pallidus; BST: brain stem; HIP: hippocampus; AMY: amygdala; NAc: nucleus accumbens; DIE: diencephalon* ***(b)*** *Visualization of the first PC*

using a volumetric representation of the brain ***(c)****. We computed a metric of "FC change" within each resting state network (RSN) by computing the change of* v *(principal eigenvector of the sliding-windows FC) across adjacent time windows (left). For each RSN, we record an "FC jump" whenever the change of* v *is in its 5th upper percentile (middle; blue circles). We then compute conditional probabilities of observing jumps in each RSN, conditioned on concurrent jumps in other RNSs (right).*

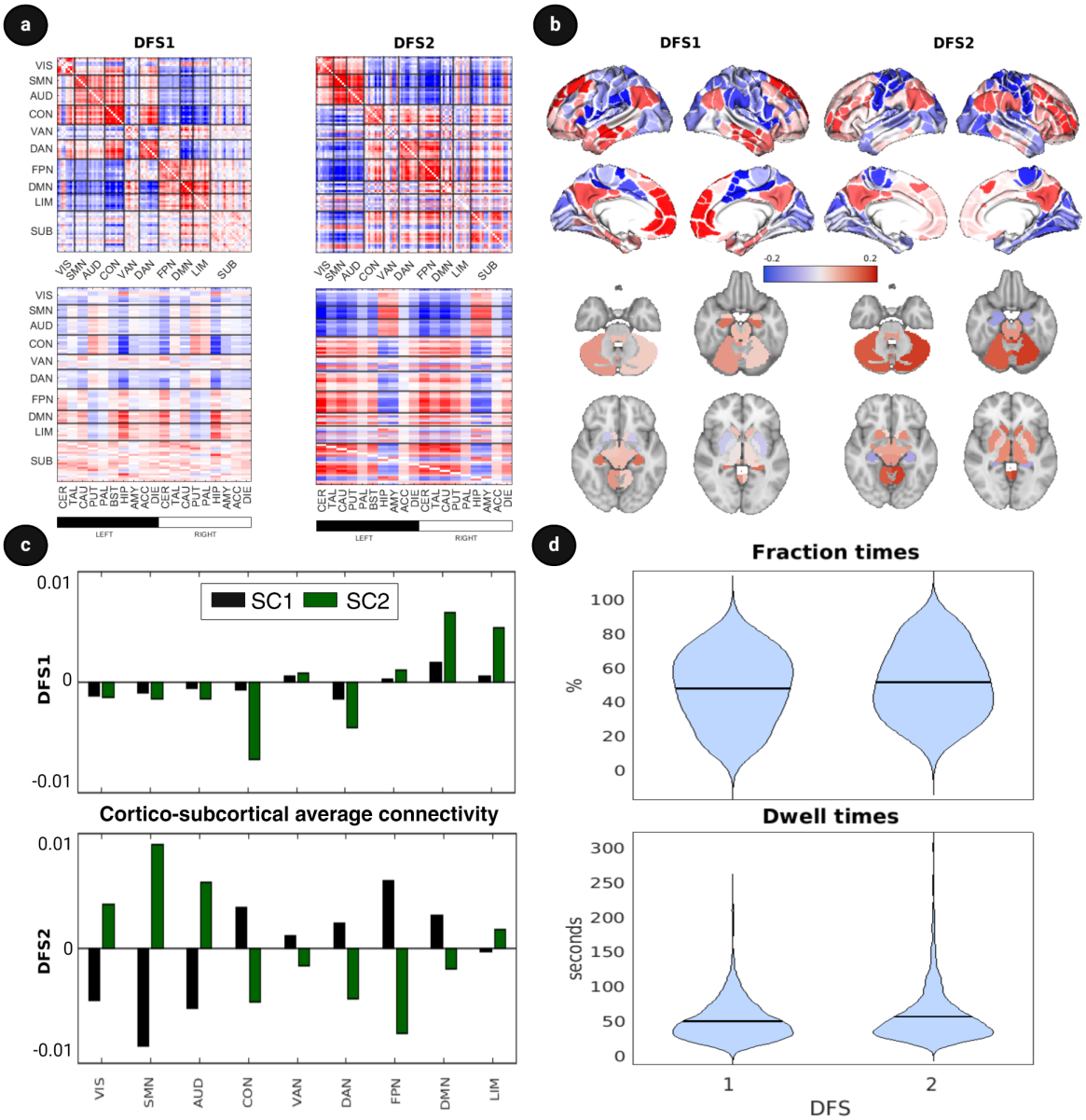

Fig. 3. DFS analysis. (a) *Matrix representation of the Dynamic Functional States displayed globally (top) and with a focus on the cortico-subcortical interactions (bottom). The most robust states observed for K=2 capture the alternating connectivity pattern observed in the Washington dataset between limbic regions (i.e., hippocampus and amygdala) and task-negative (default mode) vs. task positive (dorsal attention and sensorimotor) networks.* ***(b)*** *Volumetric representation of the Dynamic Functional States (K=2)* ***(c)*** *Average connectivity between subcortical clusters (SC1 and SC2) and cortical networks in the two most robust DFSs* ***(d)*** *Distribution of fraction and dwell times for the K=2 states. FTs/DTs*

was averaged within subjects and then plotted across subjects, resulting in box plots that display the median values (red lines), the interquartile range (upper and lower margins of the box representing the third and the first quartile respectively), the minimum and maximum values (whiskers) and eventual outliers (red crosses). VIS: visual network; SMN: sensorimotor network; AUD: auditory network; CON: cingulo-opercular network; VAN: ventral attention network; DAN: dorsal attention network; FPN: frontoparietal network; DMN: default mode network.

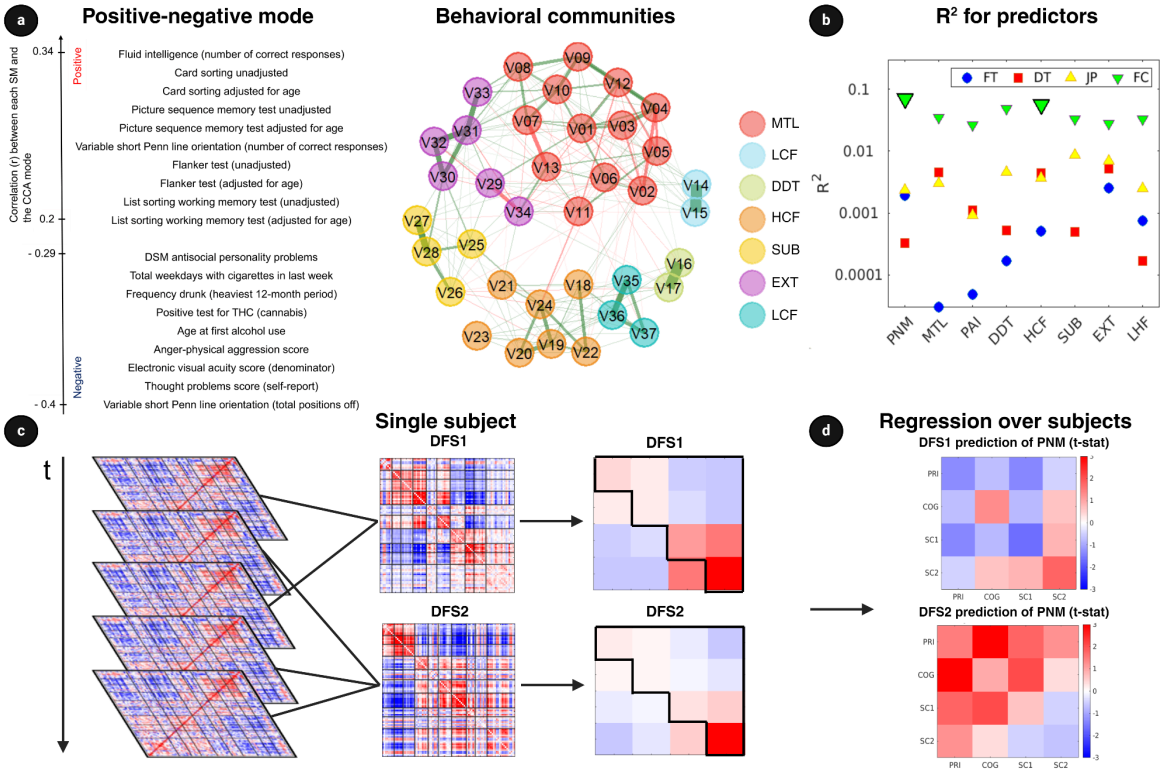

Fig.4. Functional connectivity and behavior *We investigated the impact of functional connectivity differences among individuals on behavior by carefully scrutinizing the relationships between different facets of the former and the latter through a series of Generalized Linear Models (GLMs).* ***(a)*** *In order to encompass the complexity of the multitude of behavioral and demographic indices available thanks to the HCP consortium, we employed two alternative methodologies: the first one is inspired by the work of Smith at al. (2015), which established a behavioral positive-negative mode (PNM) allowing to determine a score for each participant depending on their overall performance in a series of 150 behavioral/demographic tests (for a complete list see Supplementary Information). The second one, replicated from a recent study by Granziol et al. (2023), grouped 38 behavioral/demographic indices into 7 clusters: mental health (MTL), pain (PAI), low cognitive functions (LCF), delay discounting (DDT), high cognitive functions (HCF), substance abuse (SUB), externalizing problems (EXT). From each community we extracted a score for each subject.* ***(b)*** *We then considered several aspects of FC as predictors (fraction/dwell times, P(jump in area1\|jump in area2), individual DFSs) in an exploratory analysis to determine the most relevant representations by the means of their coefficient of determination (magnified and highlighted in black)* ***(c)*** *For each subject we separately averaged the windows assigned to DFS1 and DFS2 by the clustering procedure, resulting in*

an individual representation of the states. These representations were reduced in dimensionality to 4x4 matrices (of which we retained the upper-triangular part) averaging entries pertaining to primary networks (PRI), cognitive networks (COG) and the two subcortical components SC1/2. ***(d)*** *We show t-statistics associated with the coefficients of the linear model trying to predict the PNM from individual 4 x 4 connectivity patterns in the two DFSs.*

Discussion

Relevance of subcortical regions in whole-brain dynamics. Human neuroscience has traditionally focused on the neocortex, often neglecting the subcortical brain. There are many reasons for this 'corticocentric bias' (Parvizi et al., 2009). Superficially, it might be a consequence of technical limitations: non-invasive neuroimaging and neurostimulation techniques can probe the cortical surface much more easily than deep regions of the brain (Harrison et al., 2021): Typical protocols in fMRI and typical electrode arrangements in EEG are insufficient to detect reliable signals from subcortical regions, which may require special imaging protocols (Miletic et al., 2021) or high-density devices (Seeber et al., 2019). Detecting subcortical anatomical connections with diffusion MRI poses significant challenges (Ji et al., 2019). Transcranial magnetic stimulation can target subcortical structures only indirectly (Ulrich et al., 2018; Sydnor et al., 2022). As a consequence, knowledge of subcortical and cortical-subcortical circuits heavily relies on animal models, and much is yet to be discovered about precise structural and functional connections in humans - even for key regions such as the thalamus (Halassa and Sherman 2019; Shine et al., 2021). More profoundly, the comparatively little attention devoted to the subcortex reflects the widely held misconception that 'higher' cognitive functions in humans would entirely depend on the neocortex, and especially on frontal and association areas, which have undergone a disproportionate expansion in the human lineage and are considered the culmination of brain evolution. 'Ancient' subcortical areas instead would contribute minimally to 'higher' cognition. In fact, research in the last decade has gathered a large body of evidence showing that subcortical regions play a critical role in many advanced cognitive functions (Janacsek et al., 2022; Saban et al., 2023). Cortical evolution has not occurred 'on top' of an evolutionarily static subcortex: cortical expansion has been accompanied by a concurrent expansion and reorganization of all subcortical structures including the basal ganglia, thalamus, amygdala and cerebellum (Chin et al., 2023). According to a recent proposal (Suzuki et al., 2023), cognition would rest on a highly parallel, 'shallow' neural network architecture whereby hierarchical cortical processing is complemented by cortical-subcortical loops, and subcortical regions simultaneously integrate inputs from different levels of the cortical hierarchy.

These considerations suggest that a 'corticocentric' view ought to be abandoned, including subcortical regions in the description of large-scale brain dynamics. So far, only few studies have focused on whole-brain cortico-subcortical connectivity at rest. The majority of these works have analyzed static functional connectivity, trying to 'affiliate' subcortical structures to well-known cortical resting state networks (Habas et al., 2009; Greene et al., 2020; Li et al., 2021; Ezama et al., 2021; Barnett et al., 2021). While significantly advancing our understanding of cortico-subcortical interactions, these efforts portray a *static* coupling

between cortex and subcortex. In our previous study (FA22), we investigated *dynamic* functional connectivity and provided evidence that subcortical structures couple flexibly with cortical networks. A significant limitation of that study, however, was the use of a highly non-standard sample (including mainly stroke patients), casting some doubts on the generalizability of our findings. In the present work, we replicated the analysis of FA22 on a much larger sample of healthy young subjects, the Human Connectome Project HCP1200 data set (Smith et al., 2015). Our results provide substantial support for the main conclusions of FA22.

Existence of two main clusters of subcortical regions with different functional connectivity profiles. In FA22, the dynamic functional connectivity (FC) analysis identified two main clusters of subcortical regions. The first ('subcortical cluster 1' or 'SC1') comprised the thalamus, basal ganglia and cerebellum; the second ('subcortical cluster 2' or 'SC2'), the hippocampus and the amygdala, i.e., limbic subcortical regions. These two clusters are already distinguishable at the level of subcortical static FC (Fig. S7). Regions within the two clusters show positive FC, while negative FC is observed between the two clusters . This feature is consistently observed across different subcortical parcellations. Fine-grained parcellations of the thalamus and cerebellum confirm this 'two-block' picture with minor refinements (the posterior thalamus and the 'visual' cerebellum show only weak affiliation with SC1). In terms of (static) cortical FC, SC1 shows weakly negative static FC with primary regions (SMN, AUD, VIS) and weakly positive connectivity with associative networks (CON, DAN, VAN, FPN, DMN). On the other hand, SC2 shows a strongly positive FC with task-negative regions (DMN), a weakly positive FC with primary networks, and a weakly negative FC with associative networks. However, our dynamic FC analysis reveals that static FC 'hides' a rich dynamic picture where the two subcortical clusters couple flexibly with cortical regions. In particular, the two clusters also have anticorrelated *fluctuations* in FC. When doing a principal component analysis on sliding-window FC (sw-FC), we identified a first principal component with positive loadings on SC1 and negative loadings on SC2 (Fig. 2). This component was consistently found across different subcortical parcellations (Fig. S1). In other words, the two clusters seem to behave as 'cohesive blocks' in terms of their static and dynamic FC.

The internal cohesion of these two clusters of regions is in agreement with classical as well as recent results in the neuroscience literature. SC2 comprises regions conventionally considered part of a single system, the 'limbic system' for emotion and memory (Catani et al., 2013; Rolls et al., 2015). The tight coupling within SC1 is less straightforward to interpret. The cerebellum and basal ganglia were traditionally thought to be independent, giving complementary contributions to learning and motor control (Doya et al., 2000), and to communicate only at the cortical level. However, recent findings provided solid evidence that the two systems are reciprocally interconnected not only at the level of the thalamus (Hintzen et al., 2018), but also through more direct subcortical pathways (Bostan et al., 2018; Milardi et al., 2019). This suggests that cerebellum, basal ganglia and thalamus constitute an integrated network (Bostan et al., 2018) that acts in concert with the cortex via cortical-subcortical loops. On the other hand, the apparent antagonism between the two clusters is neither widely discussed nor reported in the literature. An exception is Chumin 2022, who investigated cortical-subcortical interactions with edge-centric functional connectivity. By clustering edges into communities, they observed that edges involving

hippocampus and amygdala have a distinct pattern from those involving striatum and thalamus (cerebellum was not considered in their study).

Cortical-subcortical synchronization in FC shifts. FA22 showed that large shifts in the connectivity of cortical regions are accompanied by large shifts in the connectivity of subcortical ones, and vice versa. Here, we confirm this observation, again by looking at the co-occurence of FC shifts in cortical networks and in the two subcortical clusters. Subcortical connectivity shifts predict cortical shifts with >75% accuracy, and vice versa (Fig 2e). This provides evidence that FC rearrangements are a phenomenon involving the cortex and the subcortex jointly. One may speculate that FC shifts are *driven* by subcortical regions, but possible mechanisms remain very hypothetical. Invasive recordings in rats have revealed that different types of subcortical activity, such as slow-frequency activity (Chan et al., 2017), ripples (Nitzan et al., 2022) and dentate spikes (Farrel et al., 2024) in the hippocampus, regular spikes (Xiao et al., 2017) and spindles (Wang et al., 2023) in the thalamus can trigger widespread cortical effects. In two cases, simultaneous electrophysiological/fMRI recording allowed observing subcortical effects on the cortical BOLD signal (Wange et al., 2023; Chan et al., 2017), in one case revealing FC changes triggered by events in the hippocampus (Chan et al., 2017). However, no such evidence has been collected in humans so far. Given the difficulty of performing causal manipulations and invasive recordings in humans, future work could at least focus on directional interactions between subcortical and cortical areas (Li et al., 2020), which could be investigated through Granger causality or effective connectivity (Allegra et al., 2024).

Alternating states of cortico-subcortical connectivity. Simultaneous shifts in cortical-subcortical FC arrangements are well captured by dynamic functional states (DFSs). Our analysis identified K=2 as the optimal number of states, and, congruently, identified two states that are consistently observed across different values of K (Fig. 3 and S5). The first state (DFS1) is characterized by a strong DAN-DMN anticorrelation, and a correspondingly antinomic pattern in the coupling of SC2 (hippocampus/amygdala) with the cortex: SC2 couples positively with the DMN and negatively with the task positive networks (DAN and primary networks). Conversely, the second state (DFS2) is characterized by a strong segregation of the primary networks from the association networks. SC2 correlates positively with primary networks and negatively with association networks, while the opposite pattern is observed for SC1. Thus, these two states capture the competitive relationship between SC1 and SC2, and their flexible coupling with task-negative vs. task-positive regions.

At present, we are hesitant to advance strong hypotheses on what drives the alternation of these states. In the light of recent literature, however, we can mention at least one possible mechanism: arousal. Many dynamic functional connectivity studies established a link between FC changes and fluctuations of arousal (Lurie et al., 2020). Based on concurrent fMRI-pupillometry or fMRI-EEG, clear evidence was given that arousal can modulate FC (Wong et al., 2013; Wang et al., 2016; Chang et al., 2016; Allen et al., 2018; Raut et al., 2021; Lee et al., 2022; Gu et al., 2022). In particular, some works related arousal variations with FC dynamics, identifying 'low-arousal' and 'high-arousal' states. Wong 2013 observed that decreases in arousal were associated with decreases in anticorrelation between the default mode and task-positive networks. Allen et al. (2018) identified a low-arousal state characterized by negative FC between the thalamus and primary networks, and reduced DAN-DMN anticorrelation. This pattern shows remarkable similarities with DFS2 in the

present study. These similarities suggest that arousal could contribute to DFS switches we observe. If arousal plays a role, then it would not be surprising to observe an involvement of subcortical regions in state switches, as the role of the thalamus in the regulation of arousal is well recognized (Redinbaugh et al., 2020). In this context, our findings would suggest that thalamus-mediated changes in arousal have a large impact on the organization or cortical and limbic connectivity.

Discrepancies between the present study and FA22. While we qualitatively reproduced the main results of FA22, there are some discrepancies between the set of DFSs found in FA22 and those found in the present work. Abrol 2017 investigated DFSs in a very large sample (n=7500) of subjects scanned at the University of New Mexico. Comparings DFSs obtained in subsamples, they reported matching sets of DFS, with typical similarities above 0.8 between the cluster centroids. Overall, this implies a considerably larger degree of consistency than the one observed between the present study and FA22. There are several possible explanations for this difference. First, the cohort studied in FA22 included stroke patients, in a percentage >50%. Stroke patients present widespread alterations of FC (Siegel et al., 2016), such as reduced interhemispheric FC and increased intra-hemispheric FC. One of the DFSs found in FA22 (DFS2) corresponded to this stereotypical 'stroke' pattern, and it is therefore unsurprising that we miss it in the present study. Another state (DFS4), characterized by anomalous degree whole-brain integration, was also over-expressed in stroke patients, and again it finds only a modest correspondence with the states of the present study. However, other differences (such as the absence of a pattern corresponding to the DFS5 in FA22) cannot be simply explained by the abundance of stroke patients in the FA22 cohort. However, the two cohorts do not only differ in terms of neurological health status: another, potentially relevant dissimilarity is due to age. The participants of FA22, being either stroke patients or age-matched healthy controls, were mostly elderly (mean age 53 years), while all HCP subjects were young (mean age 23 years). It is well known that maturation and senescence bring about large changes in the functional connectome (Cao et al., 2014). Other possible discrepancies between the results obtained on the two data sets may depend on technical issues such as different acquisition parameters, including the TR (0.7s in this study, 2s in FA22) and minor differences in preprocessing: while the preprocessing pipelines in the two studies are neatly matched, nuisance regression was performed in slightly different ways (ICA-fix in the case of HCP, regression of nuisance time series from white matter and CSF in FA22).

Surrogate time series results. The outcomes of the phase randomization (PR) analysis constrain the interpretation of dynamic functional connectivity results. By construction, PR produces surrogate data that have the same spatiotemporal correlation properties as the original data (cross-covariances at all lags are preserved), but conform to a generative model that is stationary, linear and Gaussian. Therefore, the appearance of DFSs that are virtually indistinguishable in the surrogate data (Fig. S4) implies that the observation of DFSs cannot *per se*, without further supporting evidence, be taken as evidence of non-stationary or non-linear interactions between brain regions. In particular, we cannot claim that the DFSs correspond to different stable 'attractors' of a non-linear dynamics. However, stationary, linear dynamics do not imply a fixed structure of functional coupling. Stationary models can give rise to the alternation of transient, 'metastable' patterns of synchronization between brain states (Deco et al., 2017; Cabral et al., 2022). The presence of different DFSs

indicates that inter-areal communication in the brain leads to formation and dissolution of different coupling patterns, captured by different DFSs.

The PR results are in line with previous results in the literature. Several features of fMRI time series were initially appraised as clear evidence of non-stationary or non-linear dynamics: a large variability in sw-FC (Zalesky et al., 2014), the emergence of co-activation patterns, i.e., temporally recurring spatial patterns of above-threshold activity (Liu et al., 2013), and 'events' of high-amplitude co-fluctuation, where several areas exhibit simultaneously large positive fluctuations of activity (Zamani et al., 2020). Using the HCP data set, all these features have been demonstrated also in PR surrogates, respectively by Liégeois et al. (2017; variations of sw-FC), Ladwig et al. (2022; co-activation patterns) and Matsui et al. (2022; co-fluctuation events). Abrol et al. (2017) compared DFSs results with those obtained on PR surrogates. Despite minor differences, providing feeble evidence of nonstationarity/nonlinearity, the DFSs found in the original data were very well replicated by PR surrogates. Abrol et al. (2017) concluded that the emergence of DFSs substantially depends on the lagged cross-covariance structure of the time series. As Abrol et al. (2017), we also detect some evidence of weak non-linearity, when we observe that 'FC jumps' of different areas are less synchronized than what happens in PR surrogates. This is in line with Battaglia et al. (2020), who analyzed the 'dFC speed' (distance between sw-FC matrices in contiguous sliding windows) and found that the dFC speed distribution was slightly shifted towards slower speeds in the PR null model, suggesting that PR surrogates are 'more orderly' than the original data. In synthesis, we are in full agreement with previous literature in concluding that fMRI time series are quite well captured by a stationary linear model (Nozari et al., 2024), even though a weak departure from stationarity or linearity can be detected. Future studies may investigate whether the observed structure of DFS depends on long-lag or short-lag temporal dependencies (Shinn et al., 2023). This would require fitting autoregressive models of different order, and identifying the minimal order required to reproduce the observed DFSs.

Relation between dynamic connectivity and behavior. We investigated whether dynamic FC can predict aspects of individual cognition or behavior. As discussed by Marek et al. (2022), looking for statistically reliable association between a large set of behavioral variables and inter-individual differences in brain function may require very large samples (thousands of individuals). Therefore, despite the availability of 262 variables across 15 behavioral domains in the HCP data set, we restricted attention to a few summary metrics effectively summarizing several SMs. The first was the 'positive-negative mode (PNM) of population covariation' by Smith et al. (2015), highlighting a global individual 'function outcome' associated with cognitive function, emotion regulation, and alcohol and substance use. We then considered the seven 'factors' defined by Granziol and Cona (2023) summarizing different domains (Mental Health, Externalizing problems, High-level Cognitive Functions, Basic Cognitive Functions, Substances use/abuse, Reward Delay Discounting and Pain).

We did not find a significant relationship between behavioral metric and dynamic functional state metrics such as fraction times (FT) and dwell times (DT), with all $R^2 < 0.005$. Analogously, we did not find a relation between behavior and the probabilities of cortical/subcortical FC jumps ($R^2 < 0.01$). Using the same data set, Lee et al. (2023) tested for association between the principal components of behavior and the DT/FT of co-activation patterns (CAPs). Consistently with our findings, they reported weak correlations of behavior

with DT/FT (the maximum correlation they found was R^2=0.03 between the fraction time of a specific CAP and the first behavioral PC, which roughly aligns with the PNM). These results suggest that temporal summary metrics of dynamic functional connectivity, such as the FT/DT and jump probabilities, do not significantly contribute to explaining inter-individual behavioral variability. This is possibly due to the fact that such measures do not account for individual variation in connectivity link strength. Analyzing static FC, Smith et al. (2015) could explain a large fraction of the PNM variance (R^2=0.75). However, Smith et al.'s analysis (2015) included the strength of all FC links. Liégeois et al. (2019) predicted a significant fraction of behavioral variability in the HCP data using all link strengths in the non-lagged and 1-lagged FC matrices. When considering network-averaged FC strengths associated with DFS1 and DFS2 in single individuals, we obtained significant correlations, up to R^2=0.07 for the PNM and a measure of. In particular, we see that more positive values of the PNM (generally associated with better cognitive health) correspond to a dynamic cortical-subcortical connectivity pattern, where cortex and SC1 (basal ganglia - cerebellum - thalamus) are *less integrated* in DFS1, and *more integrated* in DFS2. This suggests that healthier cognition requires an alternation of state with higher and lower cortico-subcortical integration.

Conclusion. In conclusion, our study replicates the main findings of the 2022 study by Favaretto et al. (FA22). The human brain at rest is characterized by large fluctuations in functional connectivity, with synchronized changes occurring in the cortex and the subcortex. Connectivity oscillates between states corresponding to different patterns of cortical-subcortical connectivity, captured by different dynamic functional states (DFSs). Two main groups of subcortical regions, one comprising the thalamus, basal ganglia and cerebellum, the other comprising limbic regions such as hippocampus and amygdala, show flexible coupling arrangements with task-positive and task-negative cortical regions. The mechanisms underlying synchronous cortical-subcortical connectivity changes are presently unknown and demand further investigation, possibly integrating neuroimaging results with electrophysiologic and behavioral measurements.

Bibliography

Abrol, A., Damaraju, E., Miller, R. L., Stephen, J. M., Claus, E. D., Mayer, A. R., & Calhoun, V. D. (2017). Replicability of time-varying connectivity patterns in large resting state fMRI samples. *Neuroimage*, *163*, 160-176.

Albert, N.B., Robertson, E.M., Miall, R.C., (2009). The resting human brain and motor learning. Current Biology. 19(12), 1023-1027.

Allegra, M., Gilson, M., & Brovelli, A. (2024). Directed neural interactions in fMRI: a comparison between Granger Causality and Effective Connectivity. *bioRxiv*, 2024-02.

Allen, E.A., Damaraju, E., Plis, S.M., et al., (2014). Tracking whole-brain connectivity dynamics in the resting state. Cerebral Cortex. 24(3), 663-676.

Allen, E. A., Damaraju, E., Eichele, T., Wu, L., & Calhoun, V. D. (2018). EEG signatures of dynamic functional network connectivity states. *Brain topography*, *31*, 101-116.

Barnett, A. J., Reilly, W., Dimsdale-Zucker, H. R., Mizrak, E., Reagh, Z., & Ranganath, C. (2021). Intrinsic connectivity reveals functionally distinct cortico-hippocampal networks in the human brain. *PLoS biology*, *19*(6), e3001275.

Battaglia, D., Boudou, T., Hansen, E. C., et al., (2020). Dynamic functional connectivity between order and randomness and its evolution across the human adult lifespan. NeuroImage, 222, 117-156.

Blessing, E. M., Beissner, F., Schumann, A., Brünner, F., & Bär, K. J. (2016). A data-driven approach to mapping cortical and subcortical intrinsic functional connectivity along the longitudinal hippocampal axis. *Human brain mapping*, *37*(2), 462-476.

Bostan, A. C., & Strick, P. L. (2018). The basal ganglia and the cerebellum: nodes in an integrated network. *Nature Reviews Neuroscience*, *19*(6), 338-350.

Buckner, R. L., Krienen, F. M., Castellanos, A., Diaz, J. C., & Yeo, B. T. (2011). The organization of the human cerebellum estimated by intrinsic functional connectivity. *Journal of neurophysiology*, *106*(5), 2322-2345.

Cabral, J., Castaldo, F., Vohryzek, J., Litvak, V., Bick, C., Lambiotte, R., ... & Deco, G. (2022). Metastable oscillatory modes emerge from synchronization in the brain spacetime connectome. *Communications Physics*, *5*(1), 184.

Cao, M., Wang, J. H., Dai, Z. J., Cao, X. Y., Jiang, L. L., Fan, F. M., ... & He, Y. (2014). Topological organization of the human brain functional connectome across the lifespan. *Developmental cognitive neuroscience*, *7*, 76-93.

Catani, M., Dell'Acqua, F., & De Schotten, M. T. (2013). A revised limbic system model for memory, emotion and behaviour. *Neuroscience & Biobehavioral Reviews*, *37*(8), 1724-1737.

Chan, R.W., Leong, A.T.L., Ho, L.C., et al., (2017). Low-frequency hippocampal-cortical activity drives brain-wide resting-state functional MRI connectivity. Proceedings of the National Academy of Sciences of the U.S.A. 114(33), E6972-E6981.

Chang, C., Leopold, D. A., Schölvinck, M. L., Mandelkow, H., Picchioni, D., Liu, X., ... & Duyn, J. H. (2016). Tracking brain arousal fluctuations with fMRI. *Proceedings of the National Academy of Sciences*, *113*(16), 4518-4523.

Chin, R., Chang, S. W., & Holmes, A. J. (2023). Beyond cortex: The evolution of the human brain. *Psychological Review*, *130*(2), 285.

Chumin, E. J., Faskowitz, J., Esfahlani, F. Z., Jo, Y., Merritt, H., Tanner, J., ... & Sporns, O. (2022). Cortico-subcortical interactions in overlapping communities of edge functional connectivity. *NeuroImage*, *250*, 118971.

Christensen, A. P., Golino, H., & Silvia, P. (2019). A psychometric network perspective on the measurement and assessment of personality traits. *Preprint*.

Cohen, J. R. (2018). The behavioral and cognitive relevance of time-varying, dynamic changes in functional connectivity. *NeuroImage*, *180*, 515-525.

Cole, M.W., Pathak, S., Schneider, W., (2010). Identifying the brain's most globally connected regions. NeuroImage. 49(4), 3132-48.

Deco, G., Kringelbach, M. L., Jirsa, V. K., & Ritter, P. (2017). The dynamics of resting fluctuations in the brain: metastability and its dynamical cortical core. *Scientific reports*, *7*(1), 3095.

Doya, K. (2000). Complementary roles of basal ganglia and cerebellum in learning and motor control. *Current opinion in neurobiology*, *10*(6), 732-739.

Ezama, L., Hernández-Cabrera, J. A., Seoane, S., Pereda, E., & Janssen, N. (2021). Functional connectivity of the hippocampus and its subfields in resting-state networks. *European Journal of Neuroscience*, *53*(10), 3378-3393.

Farrell, J. S., Hwaun, E., Dudok, B., & Soltesz, I. (2024). Neural and behavioural state switching during hippocampal dentate spikes. *Nature*, 1-6.

Favaretto, C., Allegra, M., Deco, G., et al., (2022). Subcortical-cortical dynamical states of the human brain and their breakdown in stroke. Nature Communications. 13, 5069.

Fischl, B., (2012). FreeSurfer. NeuroImage62, 774–781.

Fischl, B., Salat, D.H., Busa, E., Albert, M., et al., (2002). Whole brain segmentation: automated labelling of neuroanatomical structures in the human brain. Neuron. 33, 341–355.

Folstein, M.F., Folstein, S.E., McHugh, P.R., (1975). "Mini-mental state". A practical method for grading the cognitive state of patients for the clinician. Journal of Psychiatric Research. 12(3), 189-198.

Friedman, J., Hastie, T., & Tibshirani, R. (2008). Sparse inverse covariance estimation with the graphical lasso. *Biostatistics*, *9*(3), 432-441.

Glasser, M.F., Sotiropoulos, S.N., Wilson, J.A., Coalson, T.S., et al., (2013). The minimal preprocessing pipelines for the Human Connectome Project. NeuroImage. 15(80), 105-124.

Gordon, E.M., Laumann, T.O., Adeyemo, B., et al., (2016). Generation and evaluation of a cortical area parcellation from resting-state correlations. Cerebral Cortex. 26(1), 288-303.

Granziol, U., & Cona, G. (2023). Architecture and relationships among cognition, mental health and other human domains revealed by network analysis perspective. *Current Psychology*, 1-16.

Greene, D. J., Marek, S., Gordon, E. M., Siegel, J. S., Gratton, C., Laumann, T. O., ... & Dosenbach, N. U. (2020). Integrative and network-specific connectivity of the basal ganglia and thalamus defined in individuals. *Neuron*, *105*(4), 742-758.

Gu, Y., Han, F., Sainburg, L. E., Schade, M. M., Buxton, O. M., Duyn, J. H., & Liu, X. (2022). An orderly sequence of autonomic and neural events at transient arousal changes. *Neuroimage*, *264*, 119720.

Habas, C., Kamdar, N., Nguyen, D., Prater, K., Beckmann, C. F., Menon, V., & Greicius, M. D. (2009). Distinct cerebellar contributions to intrinsic connectivity networks. *Journal of neuroscience*, *29*(26), 8586-8594.

Halassa, M. M., & Sherman, S. M. (2019). Thalamocortical circuit motifs: a general framework. *Neuron*, *103*(5), 762-770.

Harrison, O. K., Guell, X., Klein-Flügge, M. C., & Barry, R. L. (2021). Structural and resting state functional connectivity beyond the cortex. *Neuroimage*, *240*, 118379.

Hindriks, R., Adhikari, M. H., Murayama, Y., Ganzetti, M., Mantini, D., Logothetis, N. K., & Deco, G. (2016). Can sliding-window correlations reveal dynamic functional connectivity in resting-state fMRI?. *Neuroimage*, *127*, 242-256.

Hintzen, A., Pelzer, E. A., & Tittgemeyer, M. (2018). Thalamic interactions of cerebellum and basal ganglia. *Brain Structure and Function*, *223*, 569-587.

Hutchison, R.M., Womelsdorf, T., Allen, E.A., et al., (2013). Dynamic functional connectivity: promises, issues and interpretations. NeuroImage. 80, 360-378.

Hwang, K., Bertolero, M. A., Liu, W. B., & D'Esposito, M. (2017). The human thalamus is an integrative hub for functional brain networks. *Journal of Neuroscience*, *37*(23), 5594-5607.

Janacsek, K., Evans, T. M., Kiss, M., Shah, L., Blumenfeld, H., & Ullman, M. T. (2022). Subcortical cognition: the fruit below the rind. *Annual Review of Neuroscience*, *45*, 361-386.

Ji, J. L., Spronk, M., Kulkarni, K., Repovš, G., Anticevic, A., & Cole, M. W. (2019). Mapping the human brain's cortical-subcortical functional network organization. *Neuroimage*, *185*, 35-57.

Jia, H., Hu, X., & Deshpande, G. (2014). Behavioral relevance of the dynamics of the functional brain connectome. *Brain connectivity*, *4*(9), 741-759.

Krauth, A., Blanc, R., Poveda, A., Jeanmonod, D., Morel, A., & Székely, G. (2010). A mean three-dimensional atlas of the human thalamus: generation from multiple histological data. *Neuroimage*, *49*(3), 2053-2062.

Ladwig, Z., Seitzman, B. A., Dworetsky, A., Yu, Y., Adeyemo, B., Smith, D. M., ... & Gratton, C. (2022). BOLD cofluctuation ‘events’ are predicted from static functional connectivity. *NeuroImage*, *260*, 119476.

Leonardi, N., Van De Ville, D., (2015). On spurious and real fluctuations of dynamic functional connectivity during rest. NeuroImage. 104, 430-436.

Lee, K., Ji, J. L., Fonteneau, C., Berkovitch, L., Rahmati, M., Pan, L., ... & Anticevic, A. (2023). Human brain state dynamics reflect individual neuro-phenotypes. *bioRxiv*.

Lee, K., Horien, C., O'Connor, D., Garand-Sheridan, B., Tokoglu, F., Scheinost, D., ... & Constable, R. T. (2022). Arousal impacts distributed hubs modulating the integration of brain functional connectivity. *NeuroImage*, *258*, 119364.

Li, R., Zhang, J., Wu, X., Wen, X., & Han, B. (2020). Brain-wide resting-state connectivity regulation by the hippocampus and medial prefrontal cortex is associated with fluid intelligence. *Brain Structure and Function*, *225*, 1587-1600

Li, J., Curley, W. H., Guerin, B., Dougherty, D. D., Dalca, A. V., Fischl, B., ... & Edlow, B. L. (2021). Mapping the subcortical connectivity of the human default mode network. *Neuroimage*, *245*, 118758.

Liégeois, R., Laumann, T. O., Snyder, A. Z. et al., (2017). Interpreting temporal fluctuations in resting-state functional connectivity MRI. NeuroImage. 163, 437–455.

Liégeois, R., Li, J., Kong, R. et al., (2019). Resting brain dynamics at different timescales capture distinct aspects of human behavior. Nature Communication. 10, 2317.

Liu, X., & Duyn, J. H. (2013). Time-varying functional network information extracted from brief instances of spontaneous brain activity. *Proceedings of the National Academy of Sciences*, *110*(11), 4392-4397.

Lurie, D. J., Kessler, D., Bassett, D. S., Betzel, R. F., Breakspear, M., Kheilholz, S., ... & Calhoun, V. D. (2020). Questions and controversies in the study of time-varying functional connectivity in resting fMRI. *Network neuroscience*, *4*(1), 30-69.

Marek, S., Tervo-Clemmens, B., Calabro, F. J., Montez, D. F., Kay, B. P., Hatoum, A. S., ... & Dosenbach, N. U. (2022). Reproducible brain-wide association studies require thousands of individuals. *Nature*, *603*(7902), 654-660.

Matsui, T., Pham, T. Q., Jimura, K., & Chikazoe, J. (2022). On co-activation pattern analysis and non-stationarity of resting brain activity. *NeuroImage*, *249*, 118904.

Milardi, D., Quartarone, A., Bramanti, A., Anastasi, G., Bertino, S., Basile, G. A., ... & Cacciola, A. (2019). The cortico-basal ganglia-cerebellar network: past, present and future perspectives. *Frontiers in systems neuroscience*, *13*, 61.

Miletić, S., Bazin, P. L., Weiskopf, N., van der Zwaag, W., Forstmann, B. U., & Trampel, R. (2020). fMRI protocol optimization for simultaneously studying small subcortical and cortical areas at 7 T. *NeuroImage*, *219*, 116992.

Nitzan, N., Swanson, R., Schmitz, D., & Buzsáki, G. (2022). Brain-wide interactions during hippocampal sharp wave ripples. *Proceedings of the National Academy of Sciences*, *119*(20), e2200931119.

Nozari, E., Bertolero, M. A., Stiso, J., Caciagli, L., Cornblath, E. J., He, X., ... & Bassett, D. S. (2024). Macroscopic resting-state brain dynamics are best described by linear models. *Nature biomedical engineering*, *8*(1), 68-84.

Palva, J. M., & Palva, S. (2012). Infra-slow fluctuations in electrophysiological recordings, blood-oxygenation-level-dependent signals, and psychophysical time series. *Neuroimage*, *62*(4), 2201-2211.

Parvizi, J. (2009). Corticocentric myopia: old bias in new cognitive sciences. *Trends in cognitive sciences*, *13*(8), 354-359.

Pons, P., & Latapy, M. (2005). Computing communities in large networks using random walks. In *Computer and Information Sciences-ISCIS 2005: 20th International Symposium, Istanbul, Turkey, October 26-28, 2005. Proceedings 20* (pp. 284-293). Springer Berlin Heidelberg.

Preti, M. G., Bolton, T. A., & Van De Ville, D. (2017). The dynamic functional connectome: State-of-the-art and perspectives. *Neuroimage*, *160*, 41-54.

Prichard, D., & Theiler, J. (1994). Generating surrogate data for time series with several simultaneously measured variables. *Physical review letters*, *73*(7), 951.

Raut, R. V., Snyder, A. Z., Mitra, A., Yellin, D., Fujii, N., Malach, R., & Raichle, M. E. (2021). Global waves synchronize the brain's functional systems with fluctuating arousal. *Science advances*, *7*(30), eabf2709.

Raichle, M.E., (2010). Two views of brain function. Trends in Cognitive Sciences, 14(4), 180-190.

Raichle, M. E. (2011). The restless brain. *Brain connectivity*, *1*(1), 3-12.

Redinbaugh, M. J., Phillips, J. M., Kambi, N. A., Mohanta, S., Andryk, S., Dooley, G. L., ... & Saalmann, Y. B. (2020). Thalamus modulates consciousness via layer-specific control of cortex. *Neuron*, *106*(1), 66-75.

Rolls, E. T. (2015). Limbic systems for emotion and for memory, but no single limbic system. *cortex*, *62*, 119-157.

Saban, W., & Gabay, S. (2023). Contributions of lower structures to higher cognition: towards a dynamic network model. *Journal of Intelligence*, *11*(6), 121.

Seeber, M., Cantonas, L. M., Hoevels, M., Sesia, T., Visser-Vandewalle, V., & Michel, C. M. (2019). Subcortical electrophysiological activity is detectable with high-density EEG source imaging. *Nature communications*, *10*(1), 753.

Shine, J. M. (2021). The thalamus integrates the macrosystems of the brain to facilitate complex, adaptive brain network dynamics. *Progress in neurobiology*, *199*, 101951.

Shinn, M., Hu, A., Turner, L., Noble, S., Preller, K. H., Ji, J. L., ... & Murray, J. D. (2023). Functional brain networks reflect spatial and temporal autocorrelation. *Nature neuroscience*, *26*(5), 867-878.

Siegel, J. S., Ramsey, L. E., Snyder, A. Z., Metcalf, N. V., Chacko, R. V., Weinberger, K., ... & Corbetta, M. (2016). Disruptions of network connectivity predict impairment in multiple behavioral domains after stroke. *Proceedings of the National Academy of Sciences*, *113*(30), E4367-E4376.

Smith, S. M., Beckmann, C. F., Andersson, J., Auerbach, E. J., Bijsterbosch, J., Douaud, G., ... & WU-Minn HCP Consortium. (2013). Resting-state fMRI in the human connectome project. *Neuroimage*, *80*, 144-168.

Smith, S.M., Nichols, T.E., Vidaurre, D., et al., (2015). A positive-negative mode of population covariation links brain connectivity, demographics and behavior. Nature Neuroscience. 18, 1565-1567.

Sydnor, V. J., Cieslak, M., Duprat, R., Deluisi, J., Flounders, M. W., Long, H., ... & Oathes, D. J. (2022). Cortical-subcortical structural connections support transcranial magnetic stimulation engagement of the amygdala. Sci Adv 8: eabn5803.

Suzuki, M., Pennartz, C. M., & Aru, J. (2023). How deep is the brain? The shallow brain hypothesis. *Nature Reviews Neuroscience*, *24*(12), 778-791.

Tian, Y., Margulies, D.S., Breakspear, M., et al., (2020). Topographic organization of the human subcortex unveiled with functional connectivity gradients. Nature Neuroscience. 23, 1421-1432.

Uddin, L.Q., Yeo, B.T.T., Spreng, R.N., (2019). Towards a universal taxonomy of macro-scale functional human brain networks. Brain Topography. 32(6), 926-942.

Ulrich, M., Lorenz, S., Spitzer, M. M. W., Steigleder, L., Kammer, T., & Grön, G. (2018). Theta-burst modulation of mid-ventrolateral prefrontal cortex affects salience coding in the human ventral tegmental area. *Appetite*, *123*, 91-100.

Van Essen, C.D., Smith, M.S., Barch M.D., et al., (2013). The WU-Minn Human Connectome Project: an overview. NeuroImage. 80, 62-79.

Wang, C., Ong, J. L., Patanaik, A., Zhou, J., & Chee, M. W. (2016). Spontaneous eyelid closures link vigilance fluctuation with fMRI dynamic connectivity states. *Proceedings of the National Academy of Sciences*, *113*(34), 9653-9658.

Wang, X., Leong, A. T., Tan, S. Z., Wong, E. C., Liu, Y., Lim, L. W., & Wu, E. X. (2023). Functional MRI reveals brain-wide actions of thalamically-initiated oscillatory activities on associative memory consolidation. *Nature Communications*, *14*(1), 2195.

Wong CW, Olafsson V, Tal O, Liu TT (2013) The amplitude of the resting-state fMRI global signal is related to EEG vigilance measures. Neuroimage 83:983–990.

Xiao, D., Vanni, M. P., Mitelut, C. C., Chan, A. W., LeDue, J. M., Xie, Y., ... & Murphy, T. H. (2017). Mapping cortical mesoscopic networks of single spiking cortical or sub-cortical neurons. *Elife*, *6*, e19976.

Yeo, B. T., Krienen, F. M., Sepulcre, J., Sabuncu, M. R., Lashkari, D., Hollinshead, M., ... & Buckner, R. L. (2011). The organization of the human cerebral cortex estimated by intrinsic functional connectivity. *Journal of neurophysiology*.

Zalesky, A., Fornito, A., Cocchi, L., Gollo, L. L., & Breakspear, M. (2014). Time-resolved resting-state brain networks. *Proceedings of the National Academy of Sciences*, *111*(28), 10341-10346.

Zamani Esfahlani, F., Jo, Y., Faskowitz, J., Byrge, L., Kennedy, D. P., Sporns, O., & Betzel, R. F. (2020). High-amplitude cofluctuations in cortical activity drive functional connectivity. *Proceedings of the National Academy of Sciences*, *117*(45), 28393-28401.

Supplementary Data

List of the 59 subject measures (SMs) with significant loading onto the principal axis of Smith et al. (2015), with their unique identifiers as provided by the HCP consortium:

PicVocab_Unadj, PicVocab_AgeAdj, PMAT24_A_CR, DDisc_AUC_200, SSAGA_Educ, DDisc_SV_1yr_200, DDisc_SV_6mo_200, DDisc_SV_3yr_200, LifeSatisf_Unadj, DDisc_SV_5yr_200, ListSort_AgeAdj, ReadEng_Unadj, SCPT_TN, SCPT_SPEC, ReadEng_AgeAdj, ListSort_Unadj, DDisc_AUC_40K, DDisc_SV_10yr_200, DDisc_SV_5yr_40K, PicSeq_AgeAdj, SSAGA_TB_Yrs_Since_Quit, PicSeq_Unadj, DDisc_SV_3yr_40K, DDisc_SV_1yr_40K, SSAGA_Income, Dexterity_AgeAdj, DDisc_SV_10yr_40K, Dexterity_Unadj, DDisc_SV_6mo_40K, DDisc_SV_1mo_200, FamHist_Fath_None, ProcSpeed_AgeAdj, Endurance_AgeAdj, Endurance_Unadj, DDisc_SV_1mo_40K, SSAGA_TB_Age_1st_Cig, ASR_Rule_Pct, ASR_Thot_Raw, EVA_Denom, SSAGA_TB_Still_Smoking, ASR_Thot_Pct, PercStress_Unadj, Taste_AgeAdj, ASR_Rule_Raw, Taste_Unadj, AngAggr_Unadj, Times_Used_Any_Tobacco_Today, PSQI_Score, Avg_Weekend_Cigarettes_7days, Avg_Weekend_Any_Tobacco_7days, Total_Cigarettes_7days, Avg_Weekday_Cigarettes_7days, FamHist_Fath_DrgAlc, Num_Days_Used_Any_Tobacco_7days, Total_Any_Tobacco_7days, Avg_Weekday_Any_Tobacco_7days, SCPT_FP, THC, PMAT24_A_S

List of the 38 subject measures (SMs) investigated by Granziol and Cona (2023), with their unique identifiers as provided by the HCP consortium:

AngHostil_Unadj, LifeSatisf_Unadj, PercReject_Unadj, PercStress_Unadj, SelfEff_Unadj, PSQI_Score, ASR_Witd_T, ASR_Thot_T, DSM_Anxi_T, DSM_Depr_T, NEOFAC_C, NEOFAC_N,

NEOFAC_E, PainIntens_RawScore, PainInterf_Tscore, DDisc_AUC_200, DDisc_AUC_40K, PicSeq_AgeAdj, PMAT24_A_CR, VSPLOT_TC, SCPT_SPEC, ListSort_AgeAdj, ER40_CR, ReadEng_AgeAdj, Total_Drinks_7days, Total_Any_Tobacco_7days, SSAGA_Times_Used_Illicits, SSAGA_Mj_Times_Used, AngAggr_Unadj, ASR_Rule_T, ASR_Extn_T, DSM_Antis_T, DSM_Hype_Raw, NEOFAC_A, Flanker_AgeAdj, CardSort_AgeAdj, ProcSpeed_AgeAdj, NEOFAC_O

Supplementary Figures

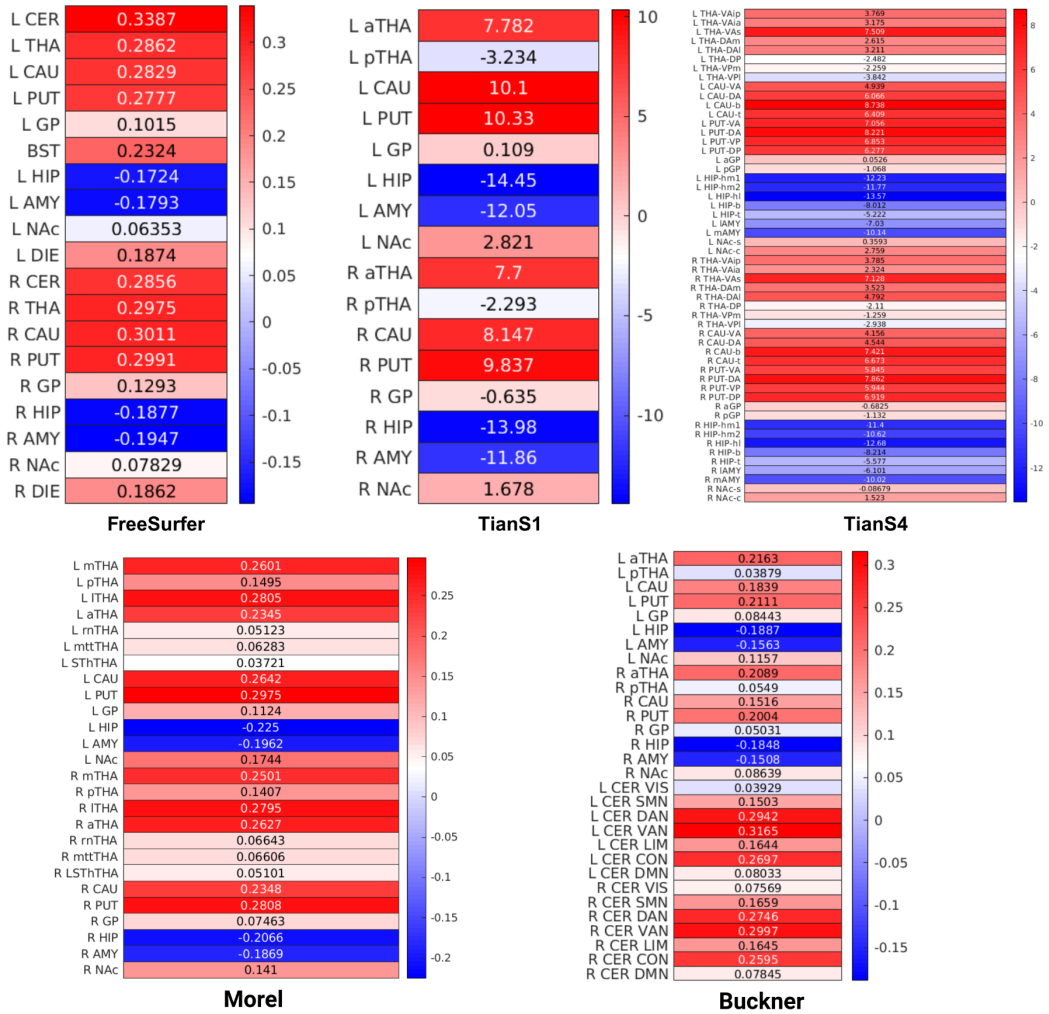

Figure S1. Subcortical clusters for different parcellations. *For each subcortical atlas, we plotted the first principal component of the time evolution of the principal eigenvector associated with the sliding-windows temporal correlation, concatenated across subjects. Each of these vectors shows the competitive relationship between two different subcortical clusters for alternative choices of subcortical parcellation* ***(a)*** *FreeSurfer subcortical atlas. Labels: CER (cerebellum), THA (thalamus), CAU (caudate nucleus), PUT (putamen), GP (globus pallidus), BST (brainstem), HIP (hippocampus), AMY (amygdala), NAc (nucleus accumbens), DIE (ventral diencephalon).* ***(b)*** *Tian S1 parcellation. Labels: same as for FreeSurfer, except aTHA (anterior thalamus), pTHA (posterior thalamus).* ***(c)*** *Tian S4*

parcellation. Labels: THA-VAip (inferior ventroanterior thalamus, posterior division), THA-VAia (inferior ventroanterior thalamus, anterior division), THA-VAs (superior ventroanterior thalamus), THA-DAm (medial dorsal anterior thalamus), THA-DAl (lateral dorsal anterior thalamus), THA-DP (dorsoposterior thalamus), THA-VPm (medial ventroposterior thalamus), THA-VPl (lateral ventroposterior thalamus), CAU-VA (ventral anterior caudate), CAU-DA (dostal anterior caudate), CAU-b (caudate body), CAU-t (caudate tail), PUT-VA (ventral anterior putamen), PUT-DA (dorsal anterior putamen), PUT-VP (ventral posterior putamen), PUT-DP (dorsal posterior putamen), aGP (anterior globus pallidus), pGP (posterior globus pallidus), HIP-hm1 (hippocampus head medial subdivision 1), HIP-hm2 (hippocampus head medial subdivision 2), HIP-hl (hippocampus head lateral subdivision), HIP-b (hippocampus body), HIP-t (hippocampus tail), lAMY (lateral amygdala), mAMY (medial amygdala), NAc-s (nucleus accumbens shell), NAc-c (nucleus accumbens core) ***(d)*** *Tian S1 + thalamic Morel parcellation. aTHA (anterior thalamus), lTHA (lateral thalamus), mTHA (medial thalamus), pTHA (posterior thalamus), rnTHA (red nucleus), mttTHA (mammillothalamic tract), SThTHA (subthalamic nucleus)* ***(e)*** *Tian S1 + cerebellar Bucker parcellation.*

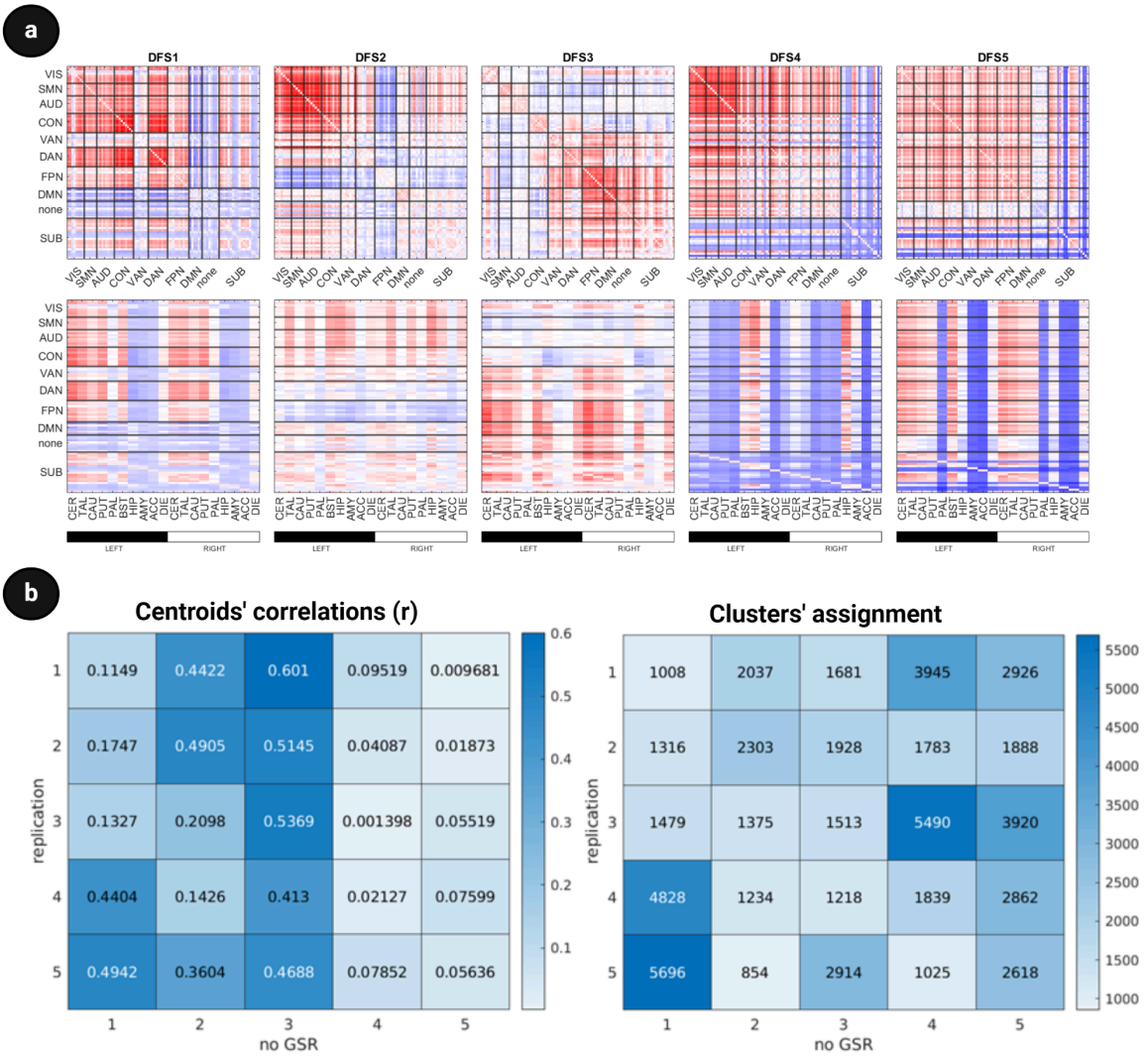

Fig. S2. Preprocessing effects: Global Signal Regression (a) *Dynamic Functional States obtained without regressing the global signal. Importantly, the aspect of the DFSs qualitatively affected by this methodological choice, which is consistent with the ongoing debate in the literature about GSR.* ***(b)*** *This is also quantitatively assessed through these confusion matrices that display correlation values between the centroids (left) and clusters' assignment with and without GSR (right).*

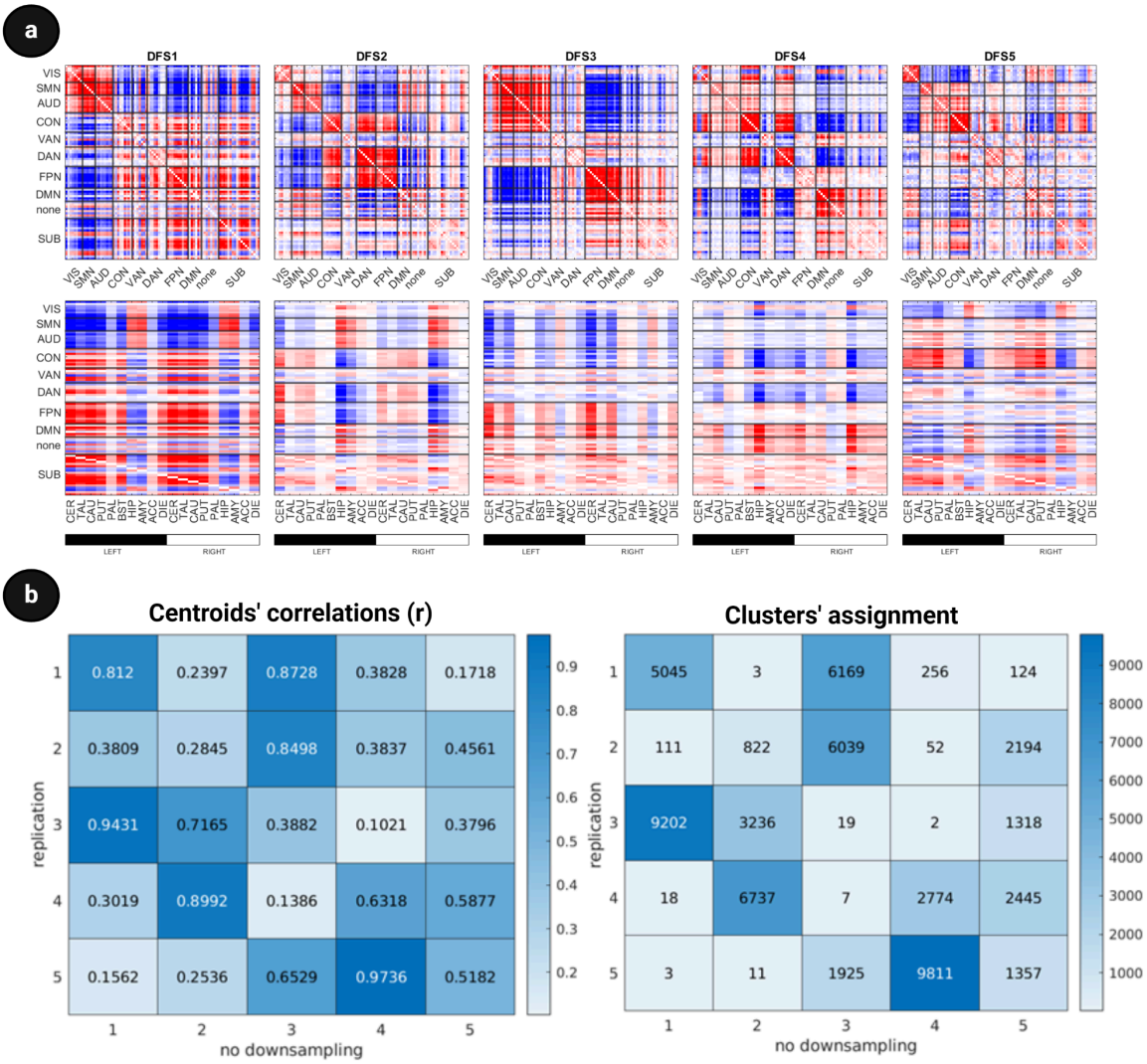

Fig. S3. Preprocessing effects: downsampling (a) *Dynamic Functional States obtained without downsampling the timeseries. Predictably, the qualitative aspect of the DFSs is not evidently affected by this methodological choice.* ***(b)*** *This is also quantitatively assessed through these confusion matrices that display correlation values between the centroids (left) and clusters' assignment with and without downsampling of the timeseries (right).*

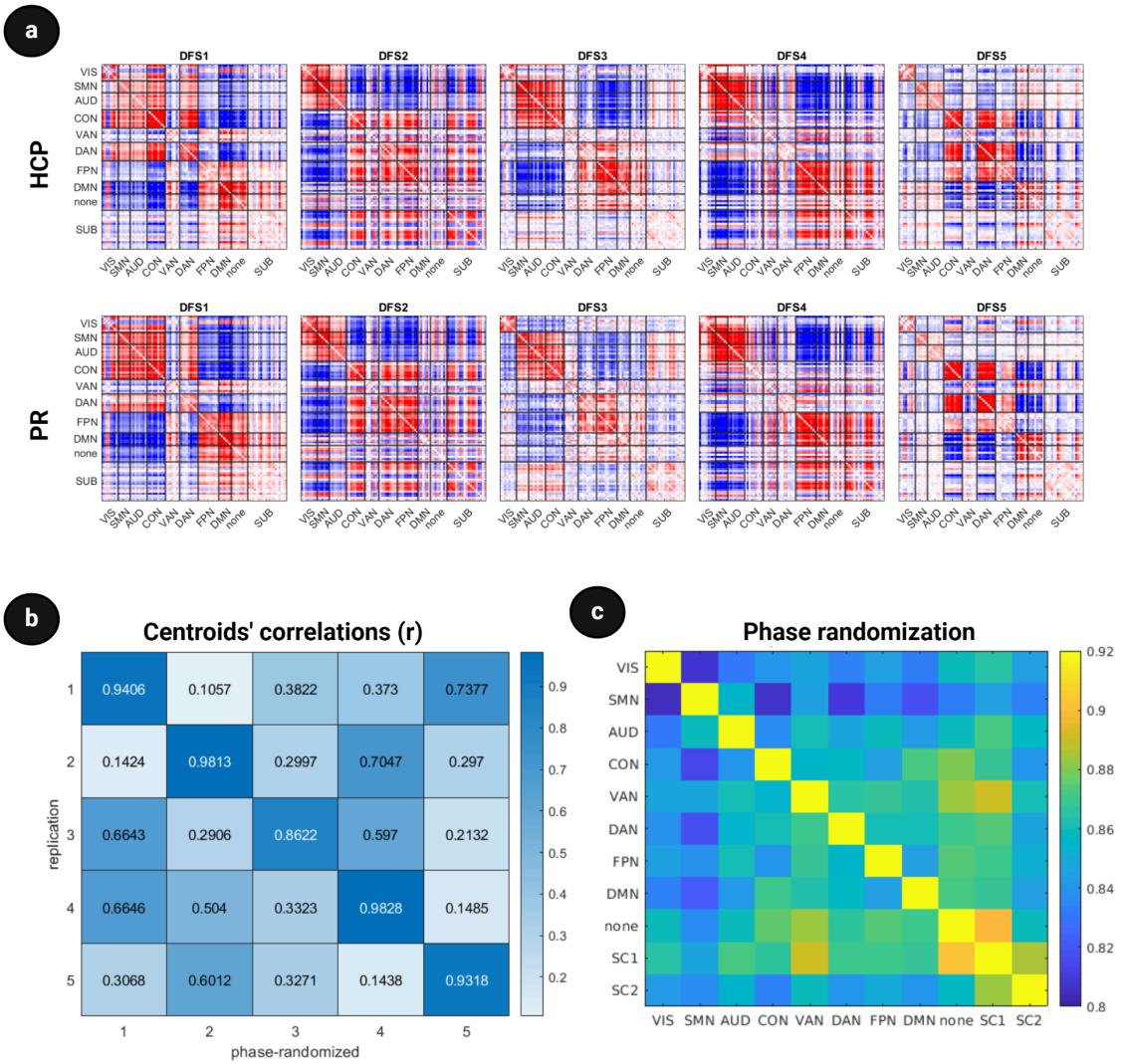

Fig. S4. Phase randomization's results (a) *Matrix representation of the cluster centroids of the K=5 dynamic functional states (DFS) found for the original HCP data (top) and for phase-randomized data (bottom). The original and PR results are barely distinguishable .* ***(b)*** *A confusion matrix with Pearson correlation values for each couple of DFS centroids between the replication study (y axis) and PR-generated data (x axis). Original and PR centroids match almost perfectly* ***(c)*** *Conditional probability matrices where we plot conditional probabilities* $P(p_i|p_j)$ *for each couple of networks, where* p_i *and* p_j *are the probabilities of a connectivity jump in the network* i *and* j *respectively. PR data qualitatively maintains the structure of conditional jump probabilities, but conditional probabilities are generally larger (KS test, P<0.05).*

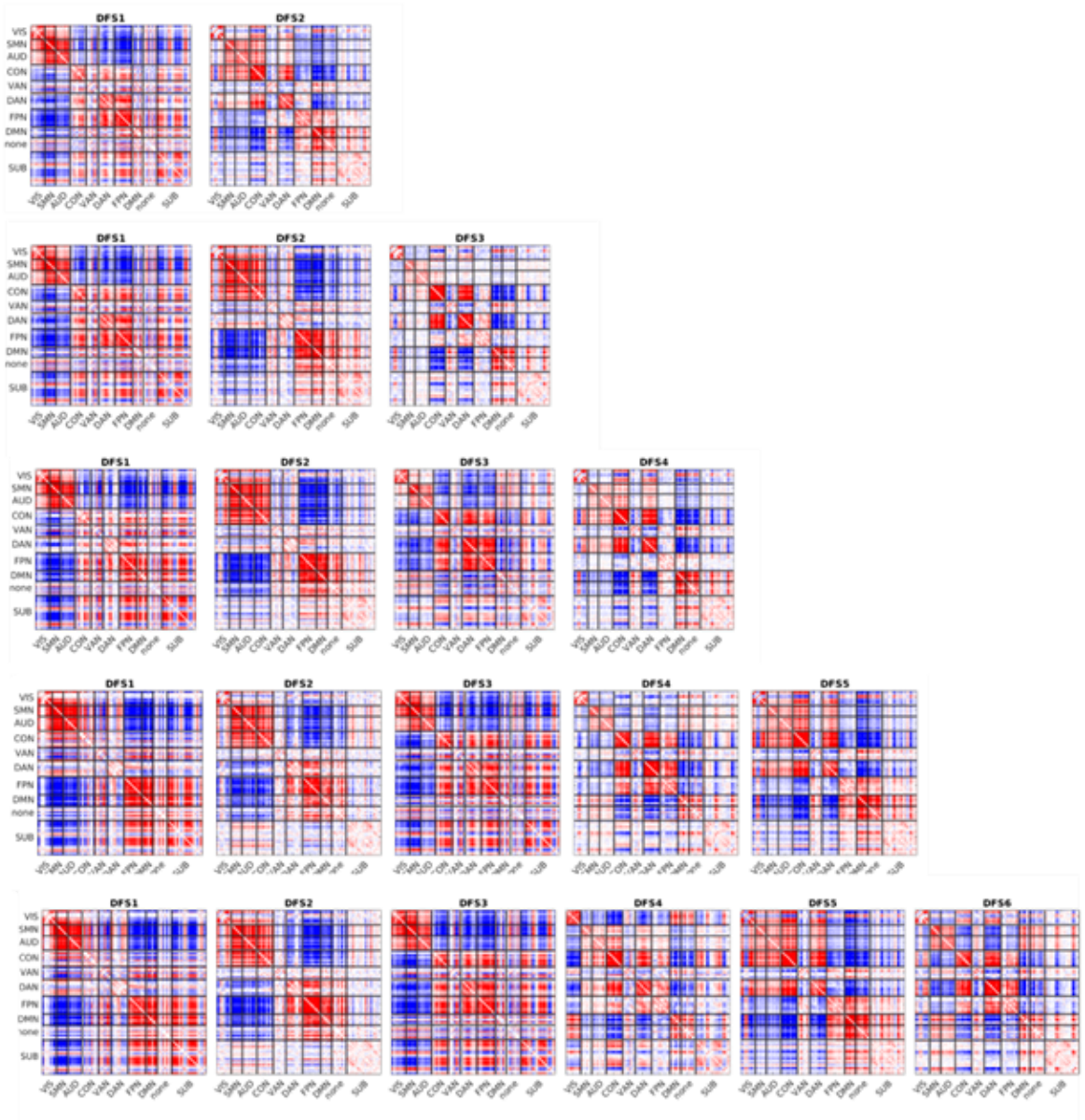

Fig. S5. Dynamical Functional States for K = 2, . . . , 6. *DFSs obtained for different values of K, from 2 to 6, with the GordonLaumann cortical atlas. In the main text we analyzed the fitness of the clustering for different values of K through the Silhouette index (fig. X). As appreciable from this figure, increasing the number of clusters led to the inclusion of new states without altering the original set present for K=2.*

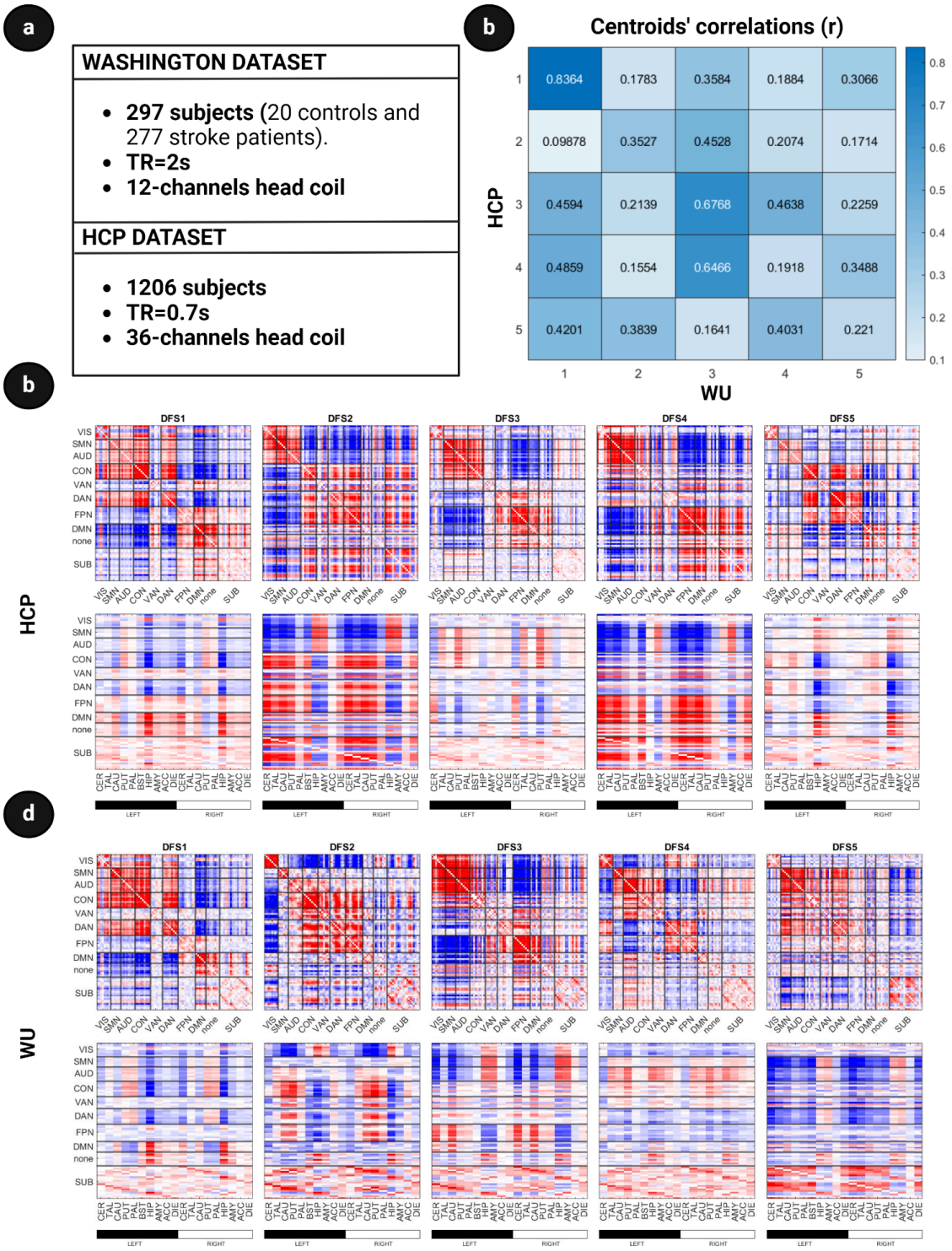

Fig. S6. Replication study. (a) *The main features of the two datasets.* ***(b)*** *A confusion matrix with Pearson correlation values for each couple of DFS centroids between the replication study (HCP) and FA22 (WU).* ***(c)*** *The cluster centroids of the K=5 dynamic functional states (DFSs) found in the HCP data set. Each centroid* v *is shown in matrix form, by plotting the matrix* $v\,x\,v^t$*.* ***(d)*** *As in* ***(c)****, but for the Washington dataset. The bottom row of* ***(c)*** *and* ***(d)*** *is a zoom in of the cortico-subcortical interaction.*

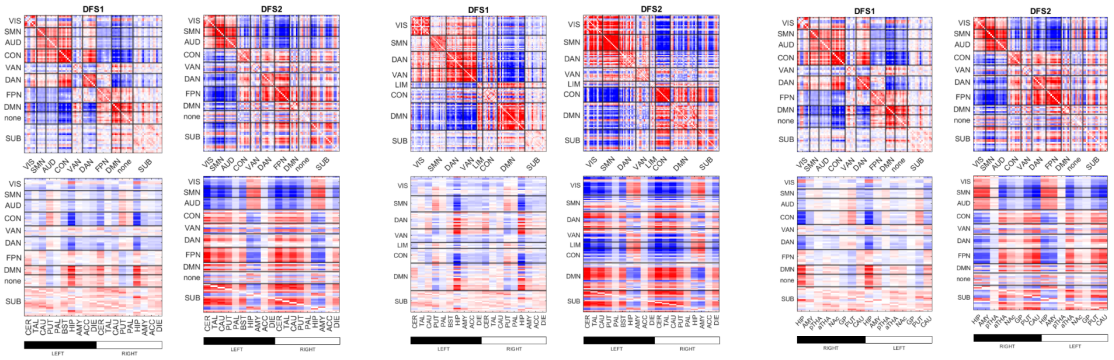

GordonLaumann+FreeSurfer **Schaefer+FreeSurfer** **GordonLaumann+TianS1**

Fig. S7. *We show the cluster centroids of the K=2 dynamic functional states (DFSs) found in the HCP data set for different choices of cortical and subcortical parcellations. Each centroid* v *is shown in matrix form, by plotting the matrix* $v \, x \, v^t$.

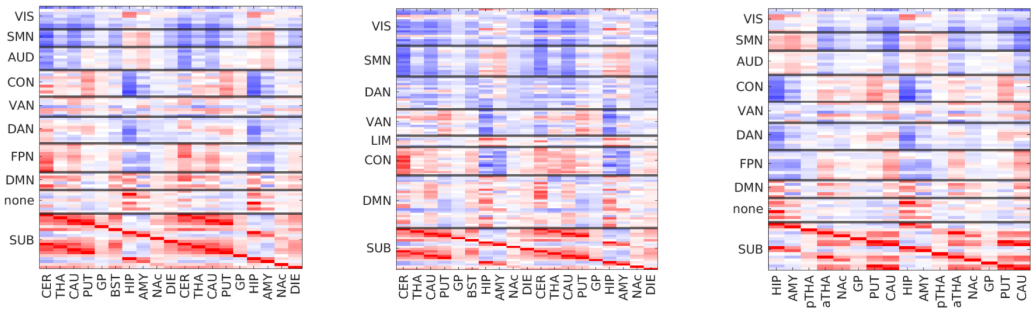

GordonLaumann+FreeSurfer **Schaefer+FreeSurfer** **GordonLaumann+TianS1**

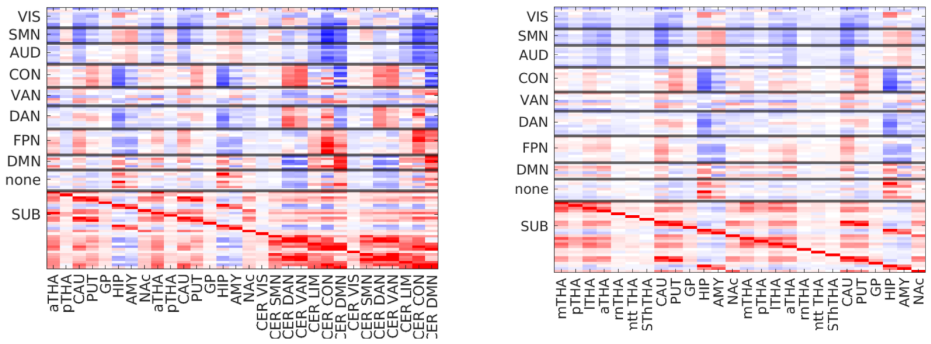

GordonLaumann+TiansS1+Buckner **GordonLaumann+TiansS1+Morel**

Fig. S8. *Subcortical static functional connectivity.*